

Investigation of Transonic Drag Computations in Aerodynamic Preliminary Analysis System (APAS)

Prepared by: Jeff Miller
Submitted to: Dr. John Olds
Georgia Institute of Technology
April 26th, 2002

TABLE OF CONTENTS

List of Figures	i
List of Tables	ii
Abstract.....	iii
Acronyms and Symbols	iv
1.0 Introduction.....	1
2.0 Transonic Drag and Wave Drag Theory	2
3.0 Approach.....	6
4.0 Methods.....	7
4.1 APAS.....	7
4.1.1 Program Description	8
4.1.2 Geometry Preparation	8
4.1.3 APAS Geometries	11
4.1.4 APAS Run Conditions and Run Setup.....	14
4.1.5 APAS Results.....	14
4.1.6 RLV Application Results	20
4.1.7 APAS “Coke-bottle” Geometry Results	24
4.2 WAVDRAG	26
4.2.1 Program Description	26
4.2.2 Geometry Input Procedure	27
4.2.3 Computation Procedure and Results	28
5.0 APAS and WAVDRAG Comparisons.....	28
5.1 Area Comparisons	29
5.2 Wave Drag Comparisons	36
6.0 Conclusions	41
7.0 Acknowledgments.....	42
8.0 References.....	43
Appendix A: WAVDRAG Input Files.....	44
Input File Description:	44
Appendix B: RLV & Trial 3b APAS Area Build-ups.....	52

List of Figures

Figure 1. Shock Wave Development.....	2
Figure 2. Typical Transonic Drag Rise.....	3
Figure 3. Equivalent Body Generation.....	4
Figure 4. Comparison of Theory with Results from Ames Laboratory Drop Tests.....	6
Figure 5. Excel Spreadsheet for Fuselage1 and Wing Addition Calculations.....	9
Figure 6. Excel Spreadsheet for Fuselage2 and Wing Addition Calculations.....	9
Figure 7. Excel Spreadsheet for Wing1 Calculations.....	10
Figure 8. Excel Spreadsheet for Wing2 Calculations.....	10
Figure 9. Trial 1 APAS Geometry.....	11
Figure 10. Trial 2 APAS Geometry.....	11
Figure 11. Trial 3 APAS Geometry.....	12
Figure 12. Trial 4 APAS Geometry.....	12
Figure 13. Trial 5 APAS Geometry.....	13
Figure 14. Trial 6 APAS Geometry.....	13
Figure 15. Trial 1 APAS Total Drag Results.....	15
Figure 16. Trial 1 APAS Results, With & Without Wave Drag.....	16
Figure 17. Trial 2 APAS Results, With & Without Wave Drag.....	17
Figure 18. Trial 3 APAS Results, With & Without Wave Drag.....	18
Figure 19. Trial 4 APAS Results, With & Without Wave Drag.....	18
Figure 20. Trial 5 APAS Results, With & Without Wave Drag.....	19
Figure 21. Trial 6 APAS Results, With & Without Wave Drag.....	19
Figure 22. APAS Geometry for Starsaber RLV	20
Figure 23. Starsaber APAS Results With & Without Wave Drag.....	21
Figure 24. APAS Geometry for Argus RLV.....	22
Figure 25. Argus APAS Results, With & Without Wave Drag.....	22
Figure 26. Stargazer APAS Results, With & Without Wave Drag.....	23
Figure 27. Stargazer APAS Results, With & Without Wave Drag.....	23
Figure 28. Trial 3b APAS Geometry.....	24
Figure 29. Trials 3 & 3b Total Drag APAS Results.....	25
Figure 30. Trials 3 & 3b Wave Drag APAS Results.....	25
Figure 31. WAVDRAG Command Screen.....	26
Figure 32. Root Airfoil of Trial 3 Configuration.....	27
Figure 33: APAS Area Build-up for Trial 1.....	29
Figure 34. WAVDRAG Area Build-up for Trial 1.....	30
Figure 35. APAS Area Build-up for Trial 2.....	31
Figure 36. WAVDRAG Area Build-up for Trial 2.....	31
Figure 37. APAS Area Build-up for Trial 3.....	32
Figure 38. WAVDRAG Area Build-up for Trial 3.....	32
Figure 39. APAS Area Build-up for Trial 4.....	33
Figure 40. WAVDRAG Area Build-up for Trial 4.....	33
Figure 41. APAS Area Build-up for Trial 5.....	34
Figure 42. WAVDRAG Area Build-up for Trial 5.....	34
Figure 43. APAS Area Build-up for Trial 6.....	35
Figure 44. WAVDRAG Area Build-up for Trial 6.....	35

Figure 45. Trial 1 Wave Drag Comparison.....36
Figure 46. Trial 2 Wave Drag Comparison.....37
Figure 47. Trial 3 Wave Drag Comparison.....38
Figure 48. Trial 4 Wave Drag Comparison.....38
Figure 49. Trial 5 Wave Drag Comparison.....39
Figure 50. Trial 6 Wave Drag Comparison.....39
Figure 51. Summary of APAS Wave Drag Results.....40
Figure 52. Summary of WAVDRAG Wave Drag Results.....40
Figure 53. APAS Argus Area Build-up.....52
Figure 54. APAS Starsaber Area Build-up.....53
Figure 55. APAS Stargazer Area Build-up.....54
Figure 56: APAS Trial 3b Area Build-up.....55

List of Tables

Table 1. UDP Analysis Runs..... 14
Table 2. WAVDRAG D/Q Results at 17 Cutting Angles 28

Abstract

The Aerodynamic Preliminary Analysis System (APAS) is often used in conceptual design studies due to its low process times and relatively good results. APAS is actually a front end to two separate analysis codes, Unified Distributed Panel (UDP) and Hypersonic Arbitrary Body Program (HABP). APAS uses UDP to analyze subsonic and supersonic runs, and HABP to analyze hypersonic runs.

Concern exists over the process by which APAS calculates transonic drag. It is common knowledge that an aircraft or spacecraft encounters a drag rise as it approaches the sound barrier, which then tapers off again once the vehicle has gone supersonic. This drag rise begins around a Mach number of 0.86, which is why most of today's passenger planes travel at or below that speed. Computer programs have been written that achieve transonic drag results equivalent to those observed in wind tunnels and drop tests. The manner in which APAS calculates drag in the transonic regime, and the accuracy of these results was the focus of this project.

It was shown that APAS deals with transonic drag rise through the addition of a wave drag term to the overall drag coefficient. Wave drag is caused by shock waves and shock-induced separation. The method by which APAS calculates wave drag was determined and compared to another code called WAVDRAG, which was also written at NASA Langley. The two programs differ slightly in that WAVDRAG calculates zero-lift wave drag, and APAS includes wave drag due-to-lift in its calculations. It was then shown that neither WAVDRAG nor APAS calculate wave drag if the freestream Mach number is less than 1.0. This yields incorrect transonic drag results, as the drag rise should begin sub-sonically. However, for the purposes of APAS, the approximation is probably "close enough." The investigation was initially performed on six simple wing-body configurations, each of which was analyzed in APAS and WAVDRAG. APAS results from the UDP analysis of three reusable launch vehicles (RLVs) designed by the Space Systems Design Lab at Georgia Tech were also examined in order to find consistency between theoretical wing-body configurations and configurations resulting from real-world applications of APAS. Finally, a simple modification was done to one of the configurations, resulting in lower wave drag.

Acronyms and Symbols

APAS	Aerodynamic Preliminary Analysis System
AR	Aspect Ratio
B	Wingspan
S_{ref}	Reference Wing Area
C_d	Total Drag Coefficient
C_{dw}	Wave Drag Coefficient
C_{dl}	Drag due to Lift Coefficient
C_{db}	Base Drag Coefficient
C_{dv}	Viscous Drag Coefficient
HABP	Hypersonic Arbitrary Body Program
NACA	National Advisory Committee for Aeronautics
NASA	National Air and Space Administration
POST	Program to Optimize Simulated Trajectories
UDP	Unified Distributed Panel
RLV	Reusable Launch Vehicle
SSDL	Space Systems Design Lab
q	Dynamic Pressure
WAVDRAG	NASA Langley Wave Drag by Area Rule Program
α	Angle of Attack
β	$\sqrt{M^2 - 1}$
μ	Mach Angle
S	total equivalent body area
L	length of equivalent body
l	component of section lift along intercept of airplane and Mach cutting plane, taken in the direction of θ .

1.0 Introduction

Aerodynamic analysis is a critical stage in the development of any new aerospace vehicle. Analysis must be performed early in the design loop and the analysis is often repeated as the design matures. Historically, aerodynamicists have had a limited number of choices regarding what computational tools and methods to use in conceptual design. Simple analysis can be done quickly using basic linear equations, but usually yield poor results. Computational Fluid Dynamics codes can yield very accurate results, but are often difficult to implement and require large amounts of time and processing capability.

The Aerodynamic Preliminary Analysis System was developed by the NASA Langley Research Center and the Rockwell International Corporation. APAS analysis can be done relatively quickly allowing multiple design iterations, and results are usually within twenty percent of actual values. Such results are good enough for conceptual design, and the speed with which they can be achieved allows designer to include aerodynamic calculations in Multi-Disciplinary Design Optimization loops.

The transonic regime is an important part of the flight envelope for many vehicles due to the large amount of drag encountered as the sound barrier is approached and broken. A vehicle must have sufficient thrust in order to overcome this drag. The thrust levels on most aerospace vehicles are determined by much more stringent requirements. The amount of thrust a high-performance aircraft requires to climb vertically or the thrust necessary for a fully fueled conceptual horizontal take-off launch vehicle to reach take-off velocity are usually both far greater than either vehicle would need to push through the transonic phase of flight. Conceptual launch vehicles that utilize turbine-based combined-cycle engines are one notable exception. Such vehicles would certainly benefit from reduced transonic drag.

Thus in conceptual aircraft/RLV design, it is important to understand the effect a vehicle's configuration has on transonic drag. The vehicle can then be designed to minimize transonic drag, which minimizes the amount of thrust required in the transonic regime, thus minimizing the amount of fuel expended. Weight reduction is the most

important factor in the conceptual design of an RLV, thus the ability to accurately calculate and understand transonic drag effects becomes important.

2.0 Transonic Drag and Wave Drag Theory

The drag rise that occurs as a vehicle nears the speed of sound is caused by the development and presence of shock waves that result in wave drag. Figure 1 shows the development of local shock waves which lead to a Mach wave as the sound barrier is broken. Local shock waves begin to develop on certain parts of an aircraft as the freestream Mach number approaches 0.85-0.9.

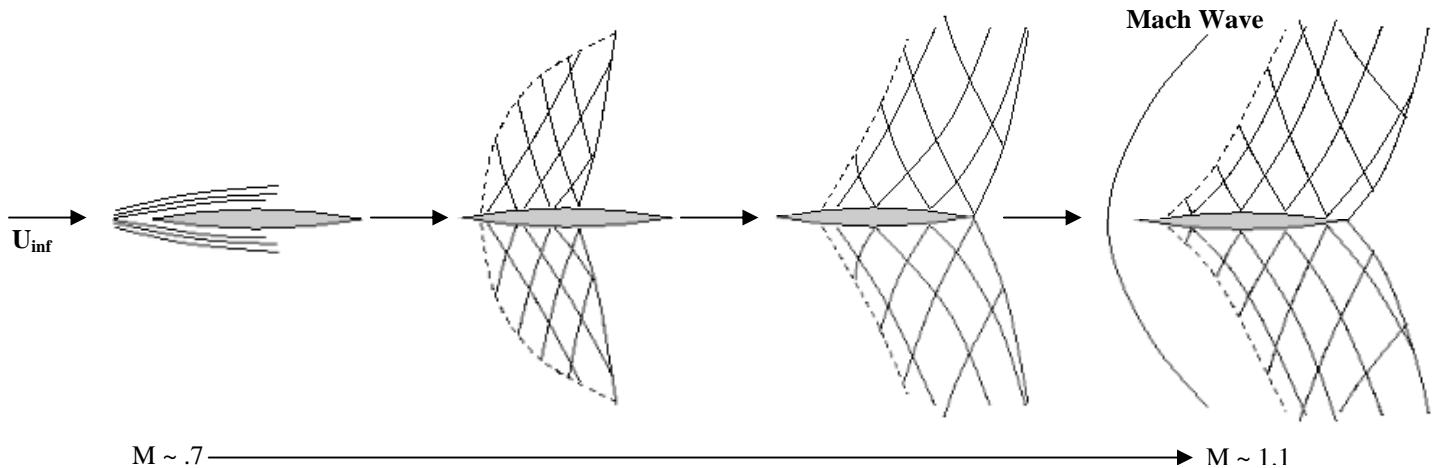


Figure 1. Shock Wave Development

These shock waves and the resulting shock induced boundary layer are the biggest contributors to transonic drag. The drag continues to increase in magnitude until the flow is fully supersonic, at which point it begins to taper off. This behavior can be seen in Figure 2, which shows a typical transonic drag rise.

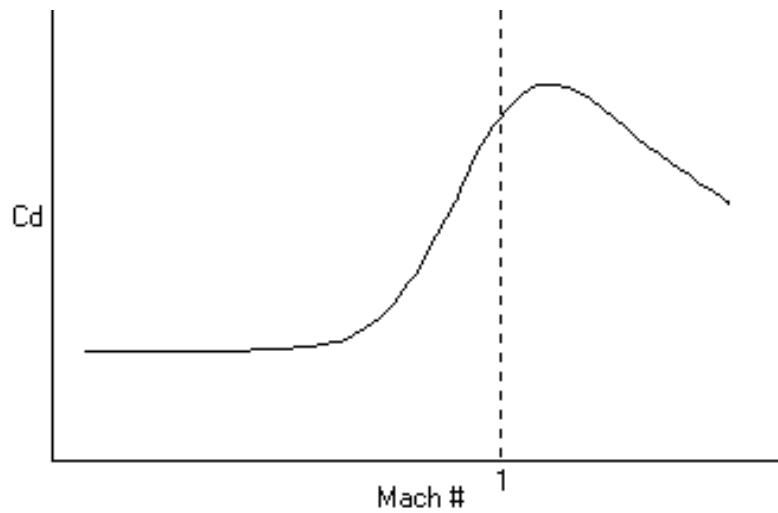


Figure 2. Typical Transonic Drag Rise

The most common method used to find the wave drag of an aerospace vehicle is known as the transonic area rule, first theorized by Wallace D Hayes. Richard T. Whitcomb at Langley Aeronautical Laboratory² developed the qualitative method by which the rule is actually used to find wave drag. The transonic area rule states that the wave drag of an aircraft is essentially the same as the wave drag of an equivalent body of revolution having the same cross-sectional area distribution as the aircraft³. This method works reasonably well in the transonic flight regime when slender body theory is applied to the equivalent body of revolution. This method fits into APAS well since the part of the program that analyzes transonic flight conditions, UDP, uses slender body theory. In order to quantitatively apply the rule, the Mach number must be greater than 1 due to limitations in linear theory, and the transonic area rule becomes the supersonic area rule.

The two programs investigated in this report differ in one important respect: WAVDRAG calculates zero-lift wave drag, while APAS calculates total wave drag (including wave drag due to lift). It is thus expected that APAS will report higher drag coefficients for each configuration than WAVDRAG.

The transonic area rule has been adapted to work at supersonic speeds. As it turns out, both APAS and WAVDRAG actually use the supersonic area rule, which is based on the transonic area rule.

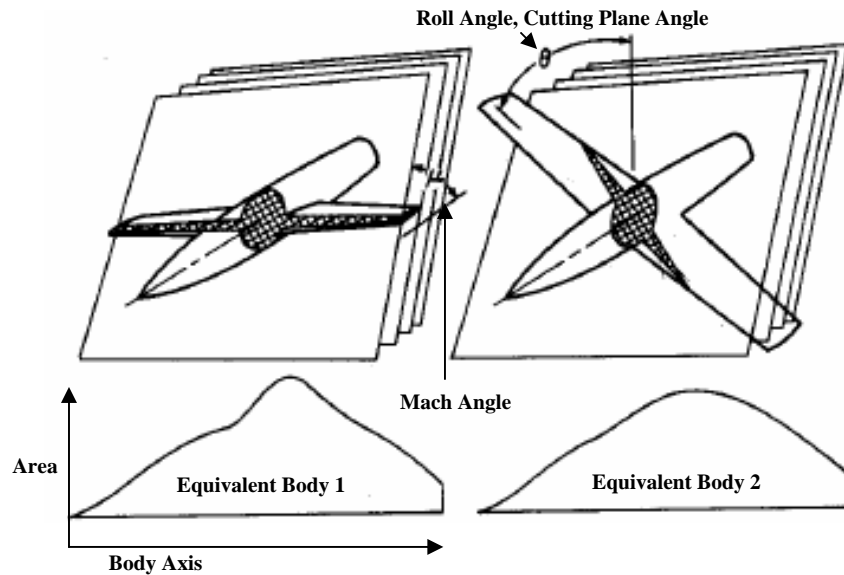


Figure 3. Equivalent Body Generation

The transonic/supersonic area rule works by passing a series of parallel cutting planes through the aircraft configuration as shown in Figure 3. In the case of the supersonic area rule, the cutting planes are inclined with respect to the aircraft axis at the Mach angle μ . This set of cutting planes can be oriented at various roll angles (θ) around the aircraft axis. An equivalent body of revolution is generated at each θ by projecting the area at each cutting plane station onto a plane that is normal to the aircraft axis. A body of revolution is constructed using these cross-sectional areas to determine the area of the body at each point along the aircraft axis. This results in a set of equivalent bodies for a particular configuration at a given Mach number. The wave drag of each equivalent body is then calculated using the von Karman formula for the wave drag of a slender body.³ The formula WAVDRAG uses to calculate zero-lift wave drag is shown below.

$$D_w = -\frac{\rho V^2}{4\pi} \int_{-x_0}^{+x_0} \int_{-x_0}^{+x_0} S''(x) S''(x_1) \ln|x - x_1| dx dx_1 \quad (1)$$

where $S(x)$ is the total cross-sectional area intercepted by a plane perpendicular to the body-axis at station x . Using a method developed by Sears, $S'(x)$ is expanded in a Fourier series to obtain a formula for the wave drag of each equivalent body :

$$x = x_0 \cos \phi \quad S'(x) = \sum A_n \sin n\phi \quad (2\&3)$$

$$D'(\theta) = \frac{\pi \rho V^2}{8} \sum n A_n^2 \quad (4)$$

The coefficients of the Fourier series are generally functions of the angle θ . The total drag of the configuration is the integrated average of all these values between $\theta = 0$ and $\theta = 2\pi$:

$$D = \frac{1}{2\pi} \int_0^{2\pi} D'(\theta) d\theta \quad (5)$$

It should be noted that the above technique used by WAVDRAG is only applicable at Mach numbers greater than 1. This formula yields wave drag of each equivalent body as a function of the area distributions of the equivalent bodies and the freestream conditions. This theory applies most accurately to aircraft that resemble bodies of revolution, thus the configurations investigated were all simple wing-body shapes with circular fuselages. APAS uses a slightly different method developed by Harris, but based on the same theory by Hayes and algorithm by Whitcomb, to calculate wave drag at lifting conditions.⁹ The far-field linear theory equation for wave drag at lifting conditions is more complicated than the zero-lift wave drag given in equation 1:

$$D_w = -\frac{\rho V^2}{8\pi^2} \int_0^{2\pi} \int_0^L \int_0^L \left[A''(x_1, \theta) - \frac{\beta}{2q} l'(x_1, \theta) \right] \left[A''(x_2, \theta) - \frac{\beta}{2q} l'(x_2, \theta) \right] \ln|x_1 - x_2| dx_1 dx_2 d\theta \quad (6)$$

Equation 6 differs from equation 1 in that wave drag is now “a function of the second derivative of the equivalent-body area distribution due to volume $A(x, \theta)$ ” as well as “a term proportional to the first derivative of the of the longitudinal distribution of lift $l(x, \theta)$ as determined by the Mach cutting planes.”⁹ It is this second contributor, the lift term, that creates the difference in results between the two programs. The total wave drag is obtained in a similar manner as the total zero-lift wave drag previously explained. A more detailed explanation of the mathematical technique used to solve equation 6 can be found in ref. 6.

Wave drag can be minimized by reducing the total cross-sectional area of the configuration at every point along the aircraft axis. Aircraft that have been optimized for

minimum wave drag usually have a fuselage with a local minimum of area in the region where the wing is attached. The increase in cross sectional area due to the wing is offset by a decrease in fuselage area. This is sometimes referred to as “coke-bottling,”² a technique which will be investigated in Section 4 of this report.

The major drawback of the linear theory used to find wave drag using slender body approximations is that it only applies to Mach numbers greater than 1. Figure 4 displays a comparison of one of Whitcomb’s experiments with his theory.

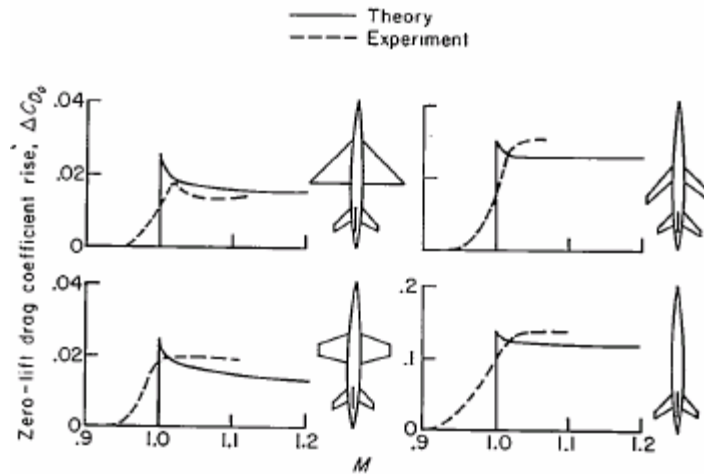


Figure 4. Comparison of Theory with Results from Ames Laboratory Drop Tests⁴

A modification of the linear area rule allows wave drag to be computed below Mach 1. The nonlinear area rule accurately predicts the correct drag rise of a configuration rather than estimating it as the linear area rule does.⁵ The nonlinear area rule:

It was found that APAS relies on the older, less exact method of “determining” transonic wave drag.

3.0 Approach

The focus of this project was the determination of how APAS accounts for the transonic drag rise. Several trial configurations would be created and the total drag of each one would be found using UDP. Various other commands in APAS would then be

used to separately calculate the subcomponents of the total drag. By studying these and comparing them to the total drag, it would become apparent which components, if any, APAS was using to account for the transonic drag rise. If a particular component was found to be the prime contributor, another program would be used to generate pertinent results with which to compare those from APAS.

4.0 Methods

Three primary computational tools were used in this investigation. The focus of the project was APAS, in which the majority of the aerodynamic computations were done. Results from APAS were compared to a code written at NASA Langley called WAVDRAG. Geometry preparation and data analysis were performed using Microsoft Excel spreadsheets.

4.1 APAS

The following equation shows the different components of total drag calculated by APAS.

$$C_{D_{tot}} = C_{D_{viscous}} + C_{D_{wave}} + C_{D_{base}} + C_{D_{lift}}$$

Each of these coefficients is calculated at each test condition when an analysis run is performed. Viscous, or skin friction drag, includes laminar/transition flow drag, turbulent flow drag, and corrections for pressure gradient effects due to the finite thickness of an actual aircraft. Wave drag is calculated using equivalent bodies of revolution (transonic area rule) according to the theory explained earlier. The third term, base drag, was omitted from the output under the assumption that it is eliminated by the vehicle's engine plume. The final term, drag due to lift, is "based on linearized potential calculations plus corrections to account for suction losses and associated vortex forces."⁶ As previously stated, the wave drag due to lift is calculated as part of wave drag, not as part of the drag due to lift computation.

4.1.1 Program Description

Transonic drag in APAS is calculated in the subsonic/supersonic portion of the program, UDP. UDP analysis is based on slender body theory and source and vortex panel methods¹. Drag calculations are performed as part of the program's background analysis, in which the user sets up specific runs, or flight conditions, at which the vehicle is then analyzed. The program generates an output file which can then be used to generate an aero-deck, which is subsequently used by the SSDL in conjunction with POST to optimize the vehicle's trajectory. This output file contains lift and drag coefficients at each specified set of flight conditions, such as angle-of-attack, altitude, and Mach number. APAS also contains commands for interactive "sub-programs" that can be run by the user in the "foreground" of the program. The commands "wave" and "visc" start two of these sub-programs that find the wave drag and viscous drag respectively at user specified flight conditions of the geometry stored in the local folder.

4.1.2 Geometry Preparation

The Excel spreadsheets shown in Figures 5 and 6 were prepared in order to facilitate geometry creation in APAS and to make rapid changes in wing size and placement without having to create multiple configurations in APAS. APAS uses command line prompts to input a configuration, one part at a time. Fuselage parts are entered as sets of streamwise coordinates, the cross sectional areas at each coordinate, and the ratio of the width of the fuselage to the height of the fuselage at each coordinate.

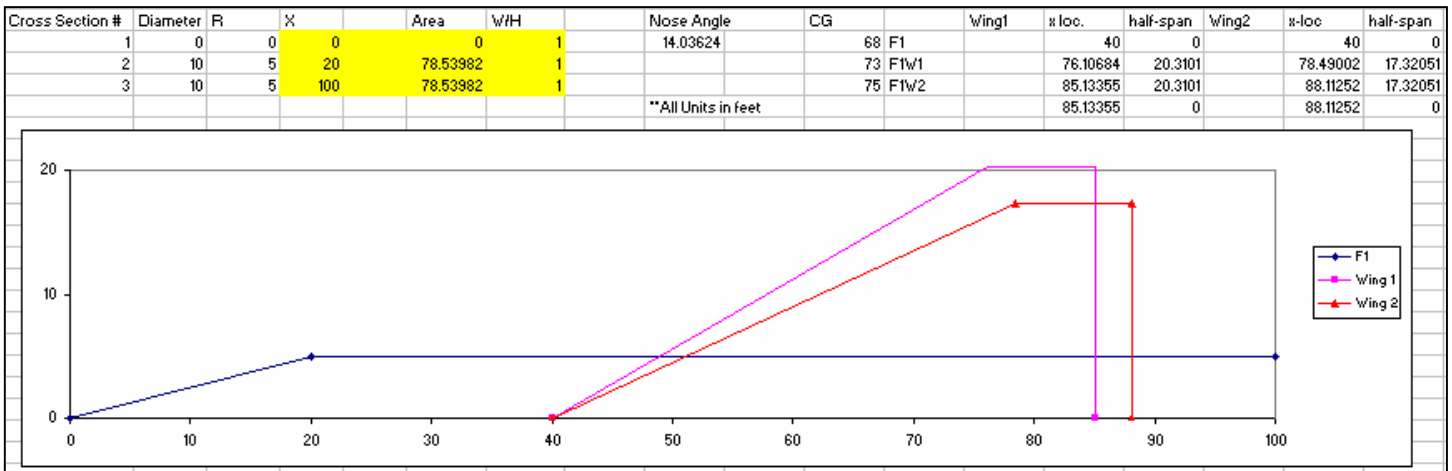


Figure 5. Excel Spreadsheet for Fuselage1 and Wing Addition Calculations

Two one-hundred ft. long fuselages were created, each with different diameters. Two wings were then created with different aspects ratios and sweep angles. This yielded a total of six configurations; two slender bodies, and four wing-body combinations. These spreadsheets were also used to determine wing placement coordinates.

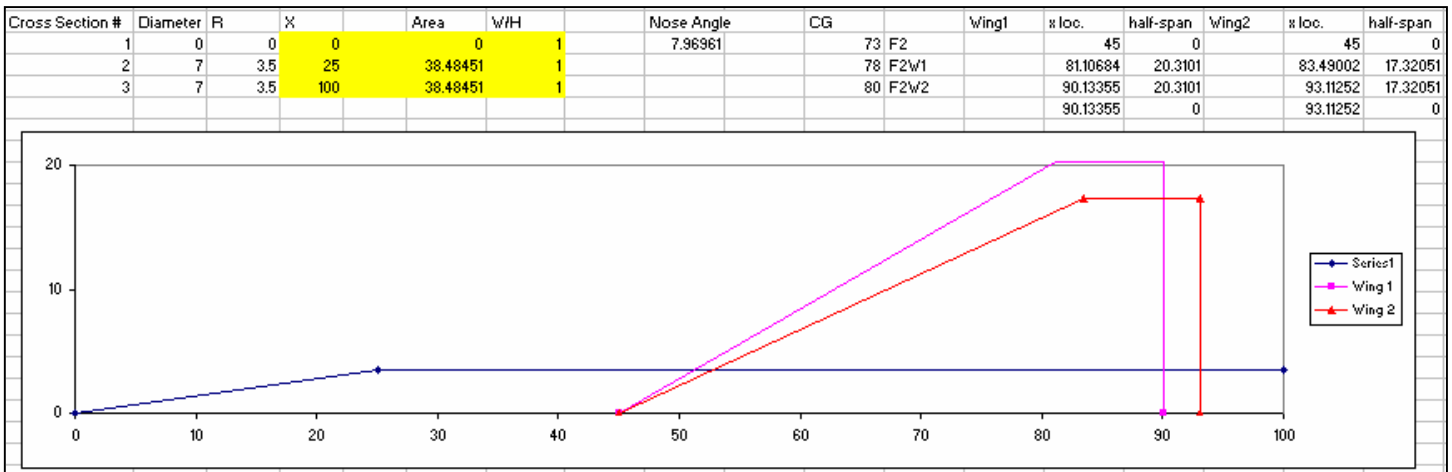


Figure 6. Excel Spreadsheet for Fuselage2 and Wing Addition Calculations

4.1.3 APAS Geometries

The geometries created for UDP analysis in APAS were intended to at least somewhat resemble those of some of the reusable launch vehicles created by the SSDL. Wing shapes and placements, as well as fuselage fineness ratios are more typical of horizontal take-off, horizontal landing RLVs than of conventional aircraft.

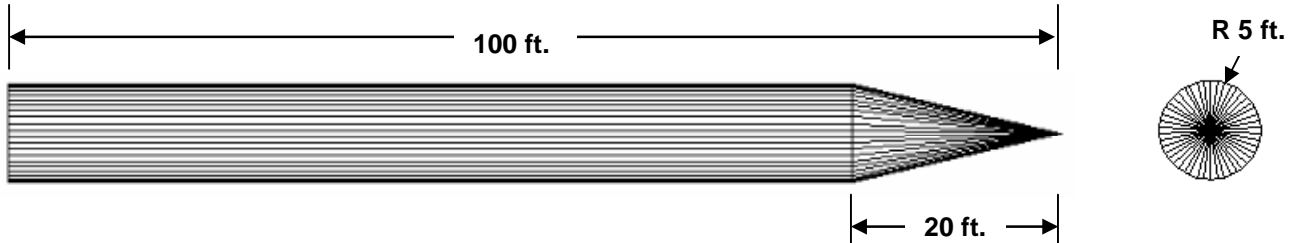


Figure 9. Trial 1 APAS Geometry

Figure 9 shows the fuselage-only (F1) geometry used for trial 1. The configuration is shown as it is displayed in APAS.

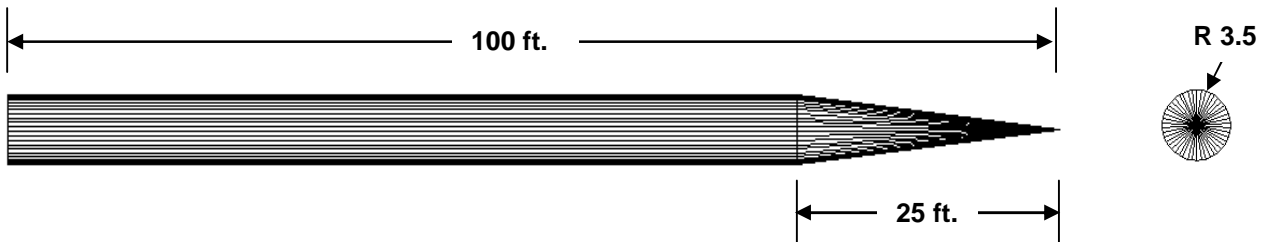


Figure 10: Trial 2 APAS Geometry

The second fuselage (F2) is shown in Figure 10. It is the same overall length as F1, but has a smaller radius and a more streamlined nosecone.

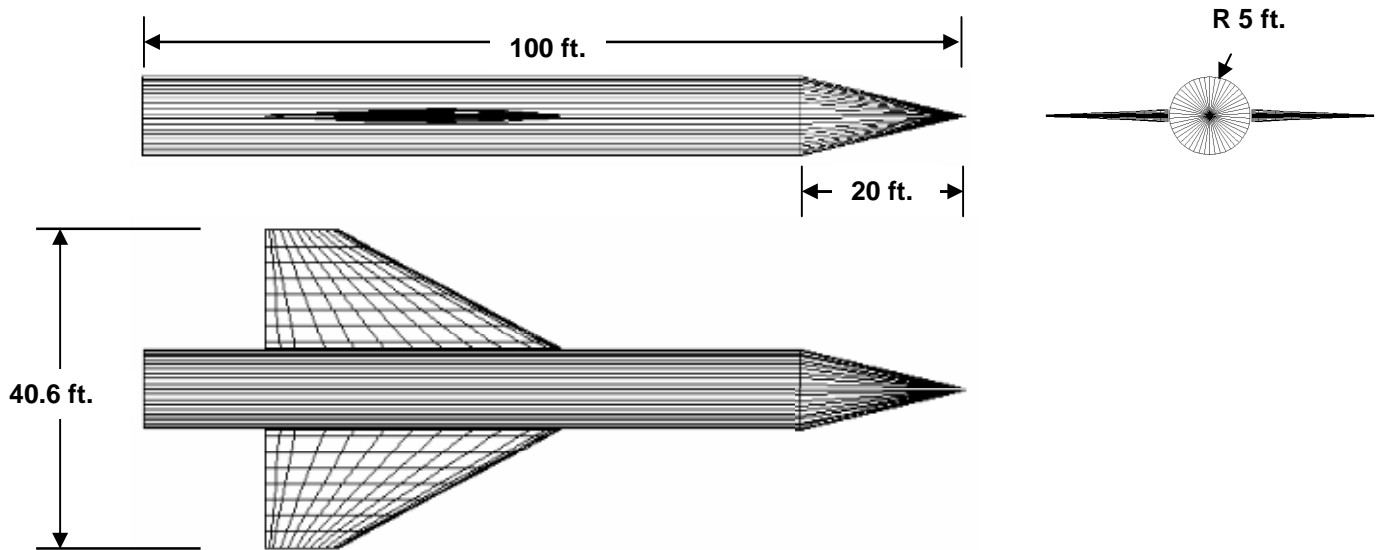


Figure 11. Trial 3 APAS Geometry

The configuration shown in Figure 11 is that of fuselage 1 with wing 1. The wing is mid-mounted on the fuselage in order to eliminate potential problems caused by the space left between wings and fuselages in APAS. Both wings 1 and 2 were constructed with NACA 65 A 0XX series airfoils, and have theoretical reference areas of 1100 and 1000 ft² respectively. The effect of “coke-bottling” the trial 3 geometry will be discussed in Section 4.1.7. Figure 12 displays the fuselage 1, wing 2 configuration.

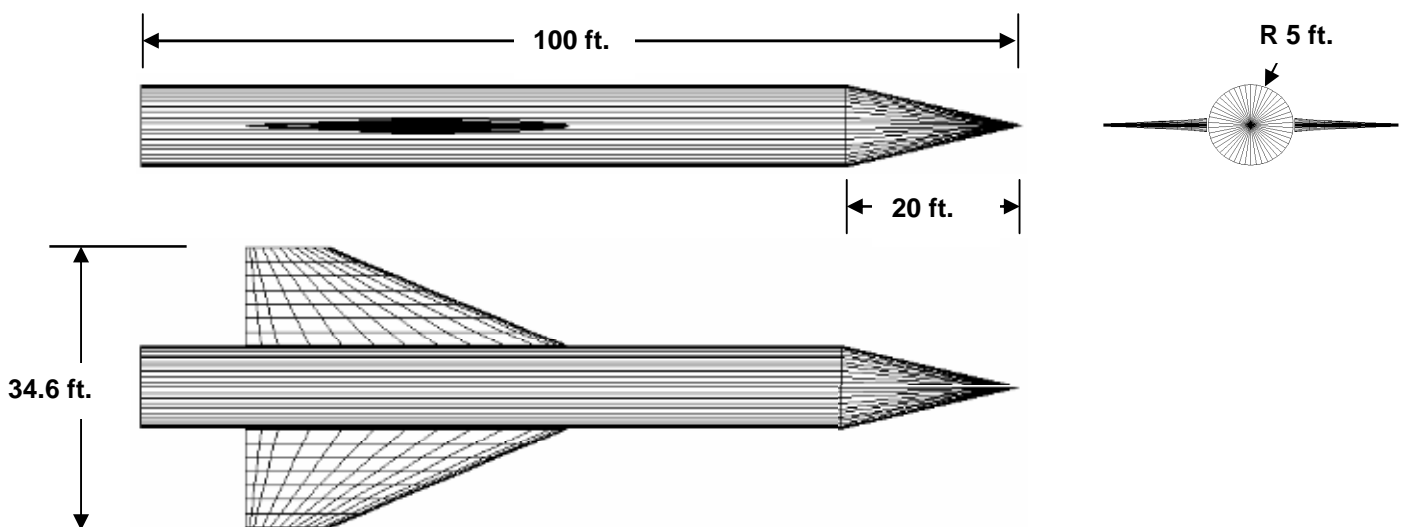


Figure 12. Trial 4 APAS Geometry

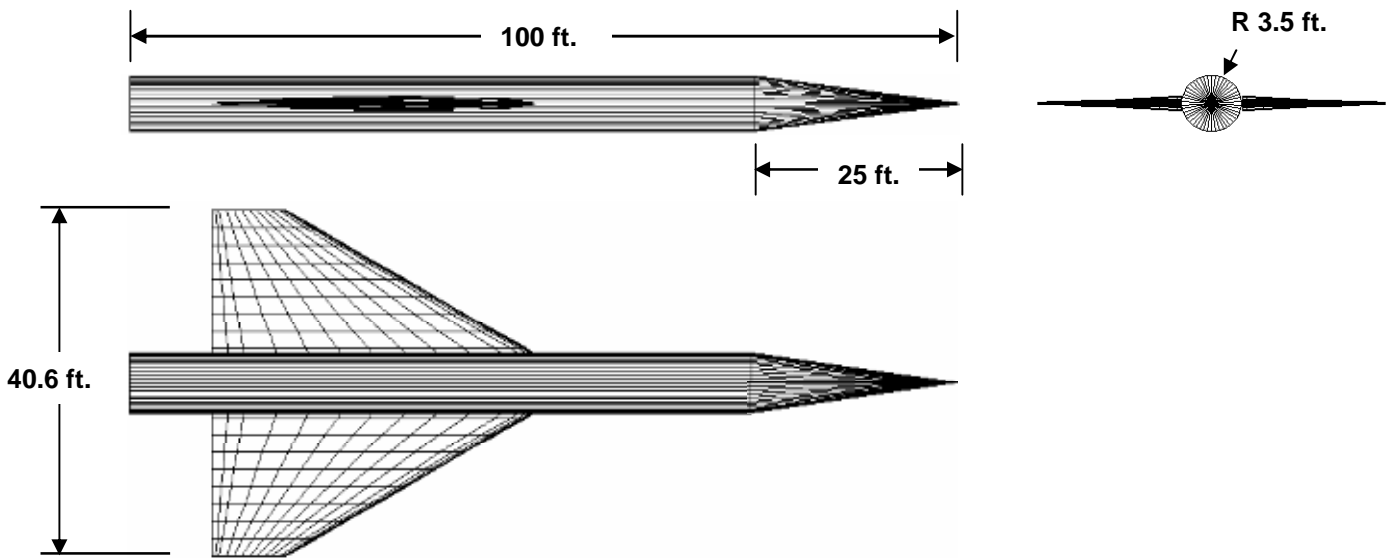


Figure 13. Trial 5 APAS Geometry

Figures 13 and 14 show the two wing-body geometries that contain the small diameter fuselage. The wing is again mid-mounted on the fuselage. The spans of these configurations are the same as those of trials 3 and 4, but there is more exposed wing due to the smaller fuselage.

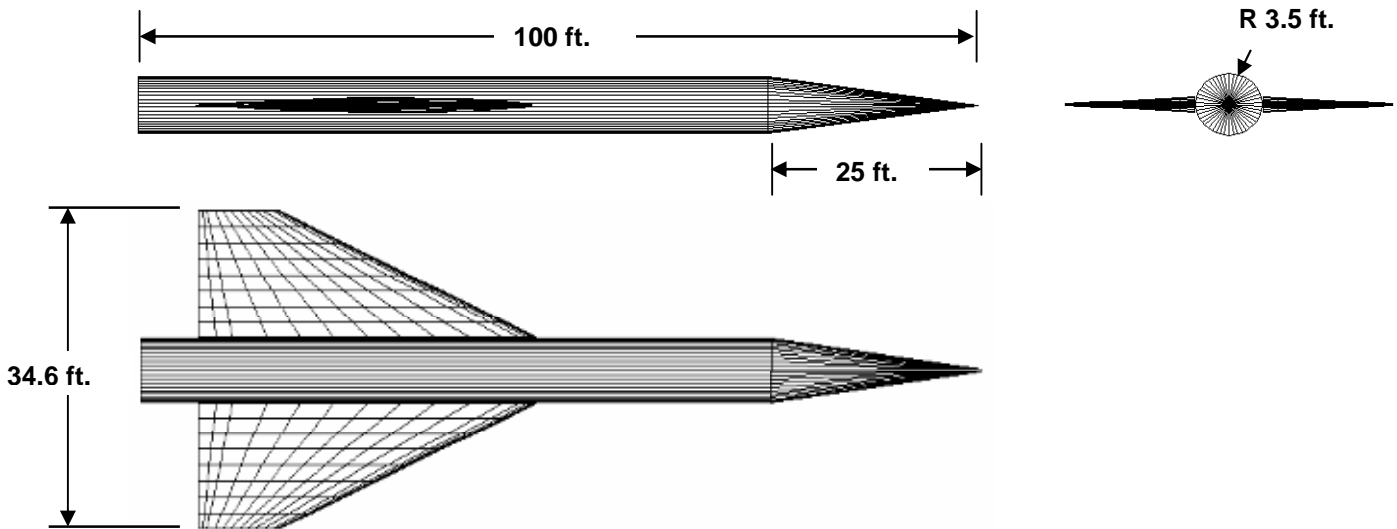


Figure 14. Trial 6 APAS Geometry

4.1.4 APAS Run Conditions and Run Setup

The flight conditions of the ten UDP runs analyzed for each trial geometry are shown in Table 2. A skin friction coefficient of 0.00025 was chosen as given in the APAS manual for “smooth matte paint, carefully applied.”

Trials 1-6 ks = .00025		
Run	Mach	Altitude (ft)
1	0.8	25000
2	0.85	25000
3	0.9	25000
4	0.95	25000
5	0.99	25000
6	1.01	25000
7	1.05	25000
8	1.1	25000
9	1.15	25000
10	1.2	25000

Table 1. UDP Analysis Runs

The runs were done at constant altitude in order to remove any variability in the results due to changes in altitude. The Mach number range of 0.8-1.2 is historically considered to be the transonic flight regime. This schedule was used for all 6 trials. Angles of attack (α) of -10, 0, and 10 degrees were analyzed. Only results at zero α will be shown, since the results did not differ greatly with α . The results at zero α also turned out to be more pertinent since it is the only α at which the wave drag subprogram in APAS generates results.

4.1.5 APAS Results

Immediately following the UDP analysis runs of the trial 1 geometry, results from APAS were viewed using “apasdat” in order to check that the analysis had been successful. From apasdat, a POST aerodeck output file was written which was then opened in Microsoft Excel for data analysis. The aerodeck includes total lift, drag, and moment coefficients at each Mach number and α . The total drag coefficients at zero α at

each Mach number were tabulated and graphed for each trial. Figure 13 shows how the total drag coefficient changes as the Mach number progresses from 0.8 to 1.2.

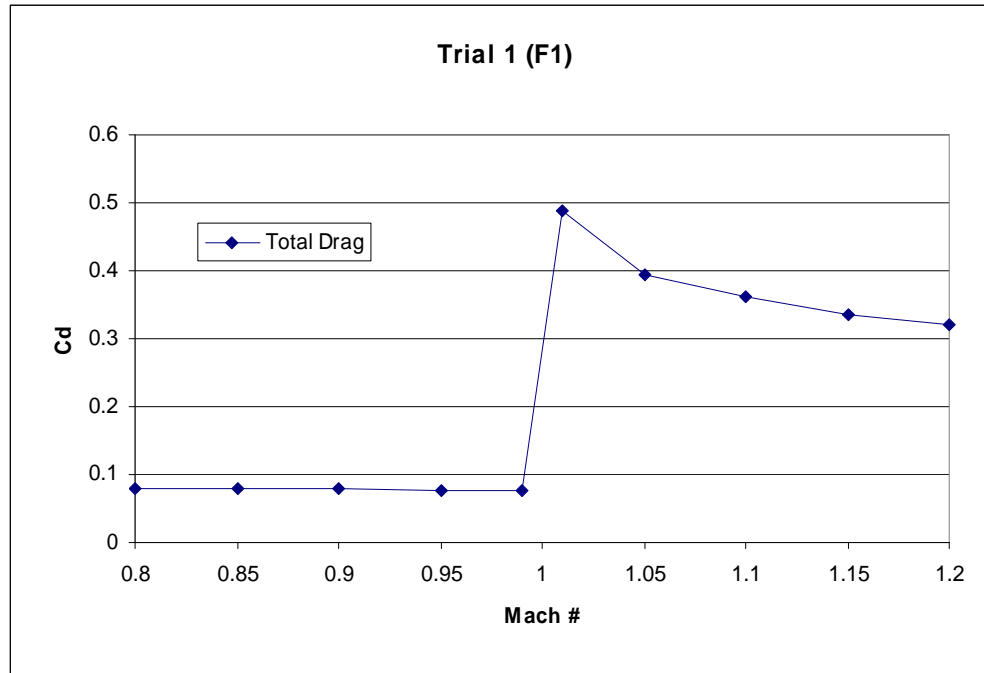


Figure 15. Trial 1 APAS Total Drag Results

It is apparent from viewing the graph that something is changing between run #5 and run #6, which have Mach numbers of .99 and 1.01 respectively. In order to determine which drag component was causing the sharp rise above Mach 1, the process of finding each of the drag subcomponents was started. The wave drag subprogram of APAS was run first. The command “wave” is entered at the APAS command prompt, and the user is asked for test Mach numbers and a reference area (wing reference area or cross sectional area of wingless body). The analysis is done on the geometry that is stored in the “local” file of APAS. For each Mach number entered, APAS generates a graph of area build-ups for various cutting angles, total D/q for each cutting angle, and a wave drag coefficient. Screenshots of the wave drag subprogram output screen will be shown in section 5 of this report. The subprogram will only return results for Mach numbers greater than 1. The wave drag coefficient was recorded for each Mach number greater than 1 at which a UDP analysis run was completed. These coefficients were than

subtracted from the total drag coefficients used to generate total drag in Figures 15 and 16. Figure 16 displays both the total drag and the results of removing wave drag from total drag.

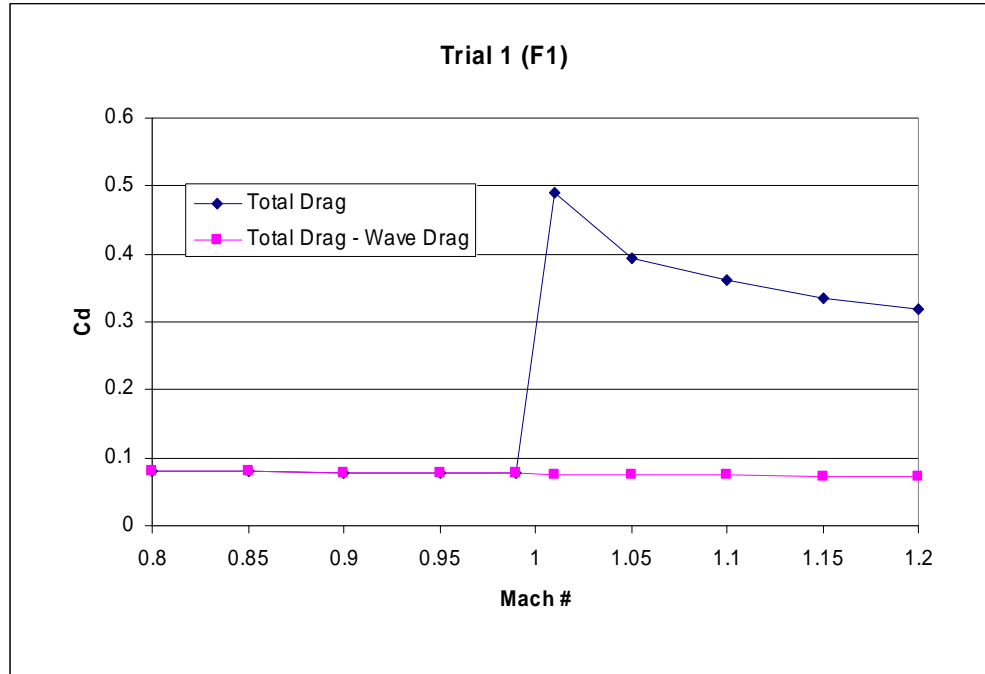


Figure 16. Trial 1 APAS Results, With & Without Wave Drag

From these results it was obvious that, at least for the geometry in trial 1, APAS was simply adding a wave drag term above Mach 1 in order to achieve a “transonic” drag rise. The plot of total drag in Figures 15 and 16 very closely resembles Whitcomb’s “theory” plots from Figure 4 on page 6 of this report. This lends credibility to the fact that APAS uses the same linear theory to calculate wave drag, and that this theory is applied through the linear area rule only above Mach 1. The same procedure was repeated for the trial 2 configuration in order to check the results using a different geometry, and to examine the affects a decrease in fuselage thickness would have. Figure 17 shows the results of both the total drag across the Mach number range, and the total drag without wave drag.

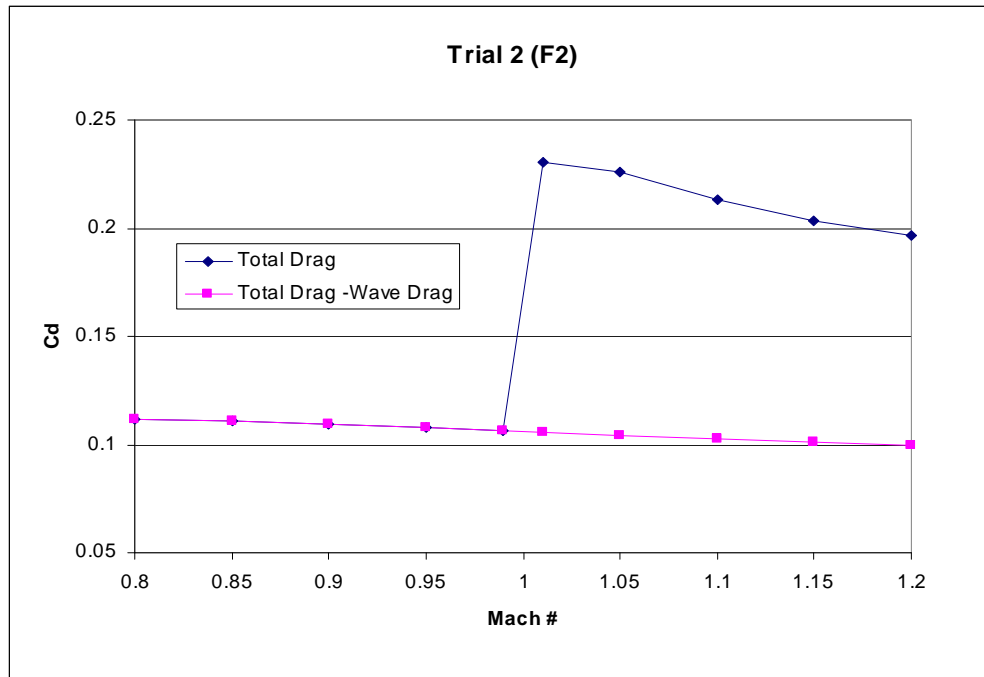


Figure 17. Trial 2 APAS Results, With & Without Wave Drag

The results from trial 2 show the same trend as those from trial 1. Again, the removal of the wave drag term from the total drag coefficient also removes the transonic drag rise. As expected, the drag coefficients are smaller than those in trial 1 since the maximum cross-sectional area of the trial 2 geometry is about fifty percent that of the trial 1 geometry.

There is a decrease in total drag without wave drag as the Mach number increases. This is a result of the flow transitioning from turbulent flow to laminar flow as freestream velocity increases. Laminar flow generates less drag than turbulent flow, so drag drops. This is evident in the results of all of the configurations analyzed and is expected.

Figures 18 and 19 show the results of the analyses done on fuselage 1 with wings 1 and 2 respectively.

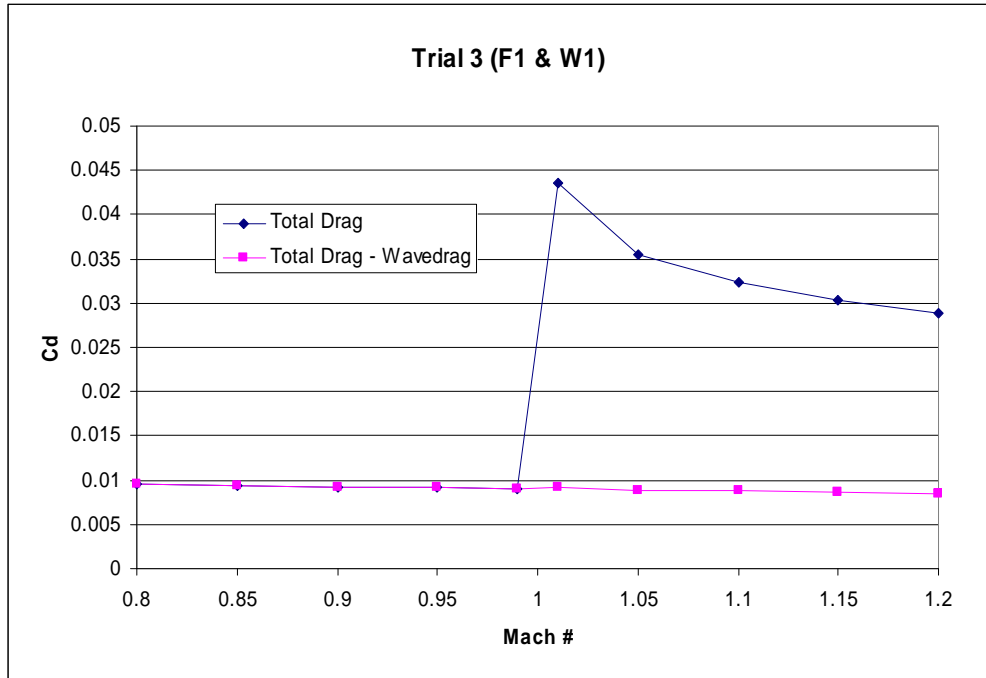


Figure 18. Trial 3 APAS Results, With & Without Wave Drag

The addition of a wing does not seem to affect the fact that there is no transonic drag rise without wave drag, nor is any wave drag generated below Mach 1. The drag coefficient for the wing 2 configuration is slightly higher than that of the wing 1 configuration, although actual drag is higher for the wing 1 configuration.

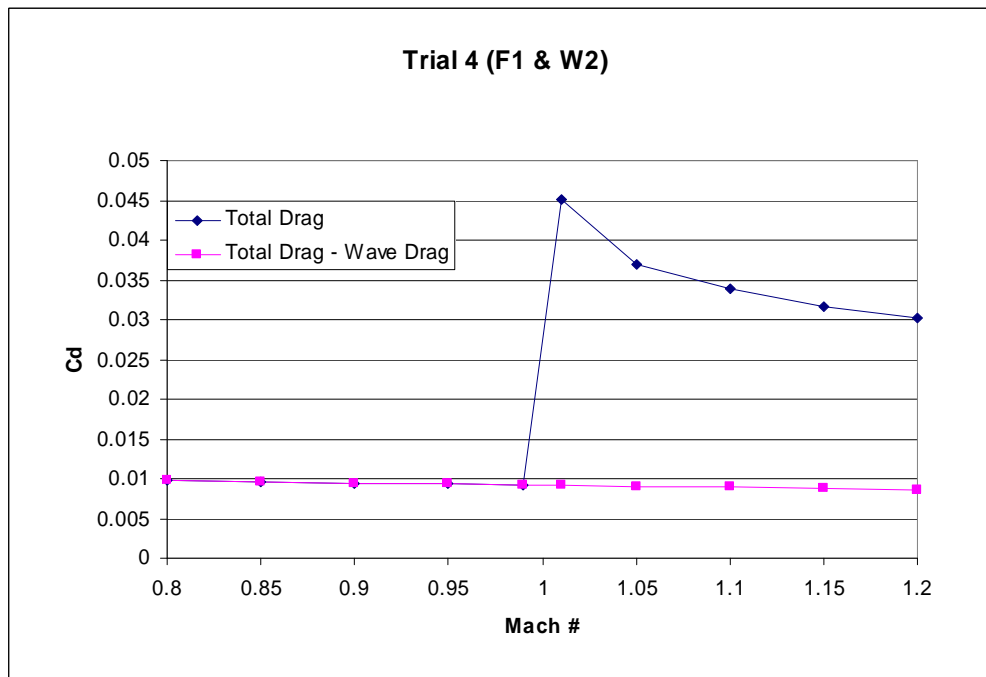


Figure 19. Trial 4 APAS Results, With & Without Wave Drag

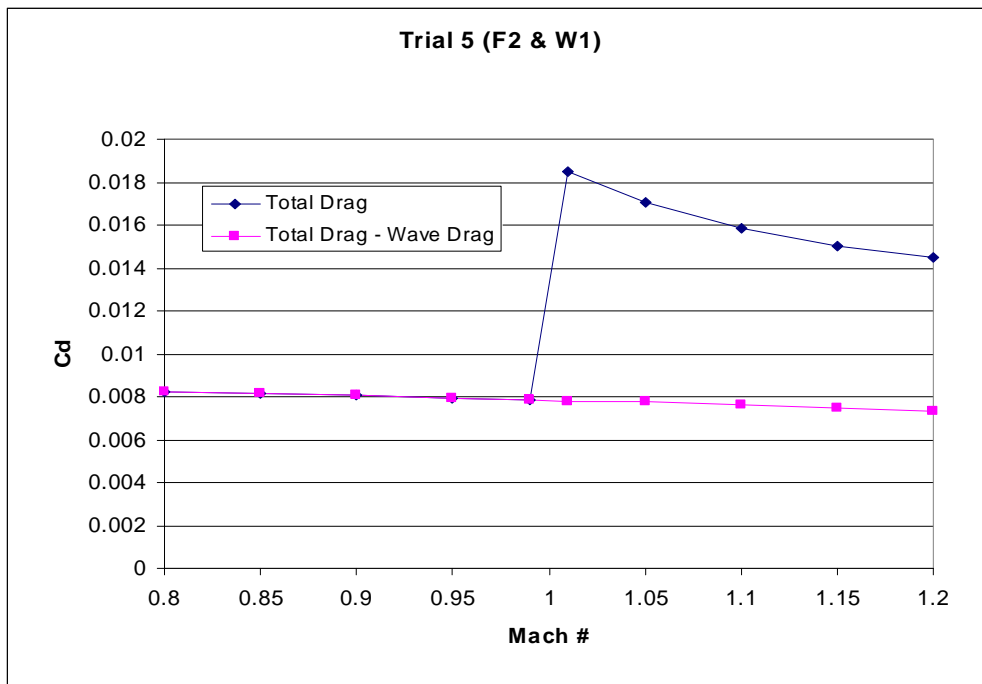


Figure 20. Trial 5 APAS Results, With & Without Wave Drag

The results of the analyses done on the addition of the two wings to the second fuselage are shown in Figures 20 and 21. The drag coefficients of both of these trials are lower than those of trials 3 and 4 as expected. The difference in wing shape has very little effect on the results.

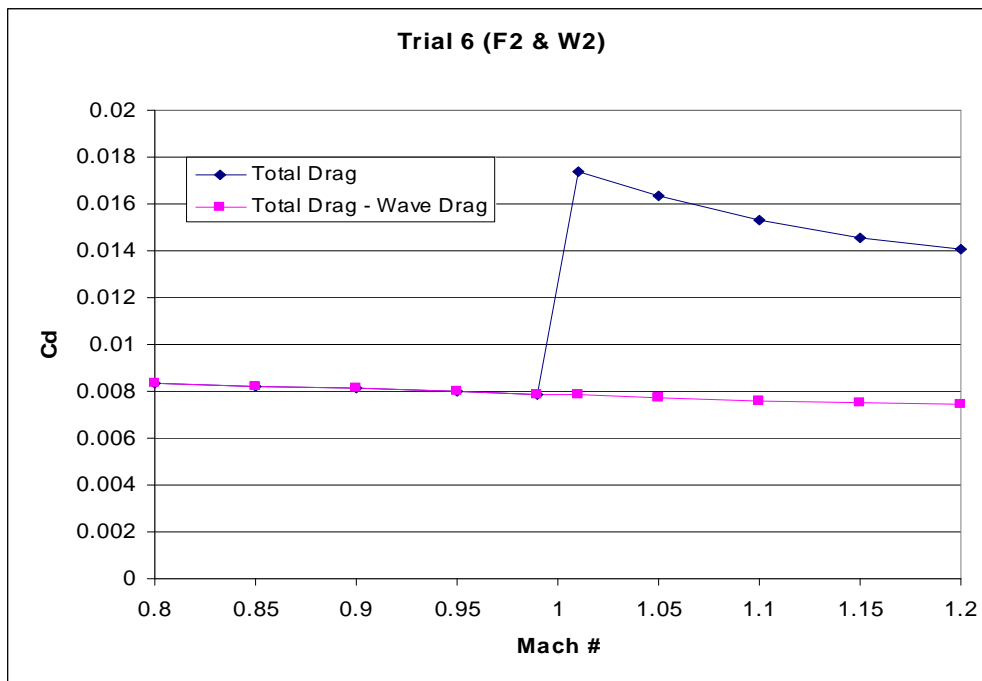


Figure 21. Trial 6 APAS Results, With & Without Wave Drag

The resulting trends of every configuration developed for this study are the same. APAS creates a transonic drag rise simply by adding a wave drag term to the total drag coefficient at flight Mach numbers greater than 1. It should again be noted that neither UDP nor the wave drag subprogram will return results at Mach 1.

4.1.6 RLV Application Results

In order to eliminate the possibility that the results were all the same due to limited configuration variety in the test cases, the aerodecks of three reusable launch vehicles designed by the Space Systems Design Lab at the Georgia Institute of Technology were examined. The wave drag subprogram was then used to determine the wave drag coefficients, using reference wing areas obtained from the RLV's respective weights and sizing spreadsheets.

The first SSDL designed vehicle studied is shown in Figure 22. Starsaber is a horizontal take-off, horizontal landing RBCC powered RLV. Theoretical reference wing area for this vehicle is 1326.9 ft².

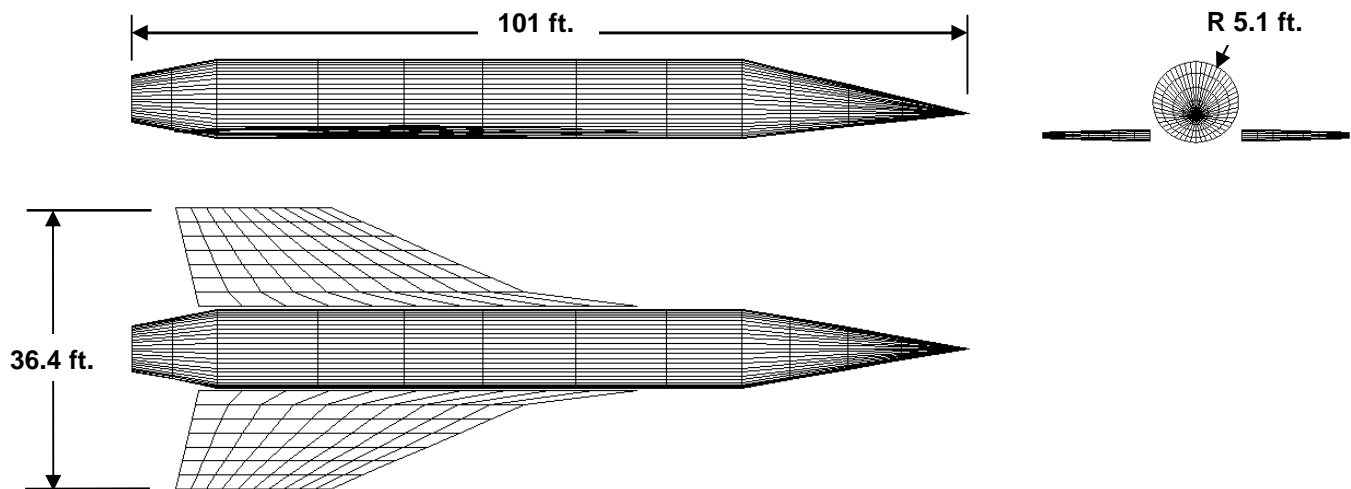


Figure 22: APAS Geometry for Starsaber RLV

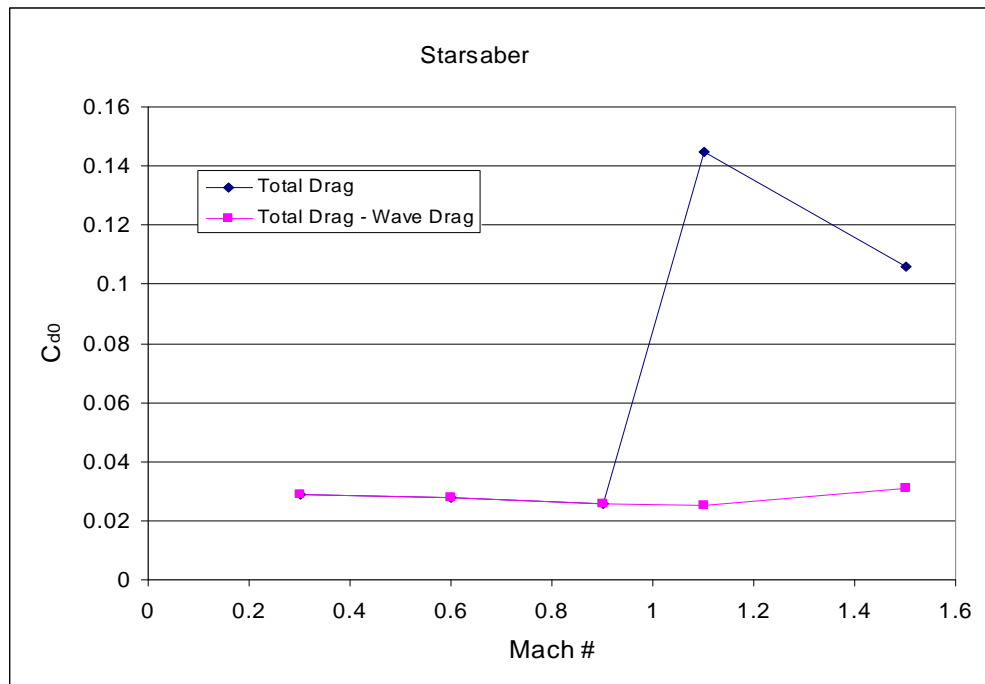


Figure 23. Starsaber APAS Results With & Without Wave Drag

Figure 23 shows the APAS drag coefficients of Starsaber. Once again, the subtraction of wave drag from total drag eliminates the transonic drag rise. A run schedule quite different from the one used for trials 1-6 was analyzed at the time of the design of Starsaber, as evident by the points in the figure. The approximation APAS makes by adding wave drag above Mach 1 works better here since the last data point before Mach 1 is Mach 0.9. Interpolation between the total drag at Mach 0.9 and Mach 1 results in a transonic drag rise, as seen in Figure 23. By properly choosing the last Mach number analyzed before Mach 1, the user can get a more realistic transonic drag rise. Total drag without wave drag seems to increase after Mach 1.1, the cause of this is difficult to determine without a more detailed analysis including a breakdown of the other contributing drag types.

The second vehicle studied was the Argus RLV. Argus and Starsaber have very similar configurations. The main difference between the two is the location of the RBCC engines. The engines on Argus are mounted directly to the fuselage on either side above the wing. Flow that would contribute to lift over this part of the wing instead goes into the engine nacelles, so a portion of the wing is removed to compensate, as shown in Figure 24.

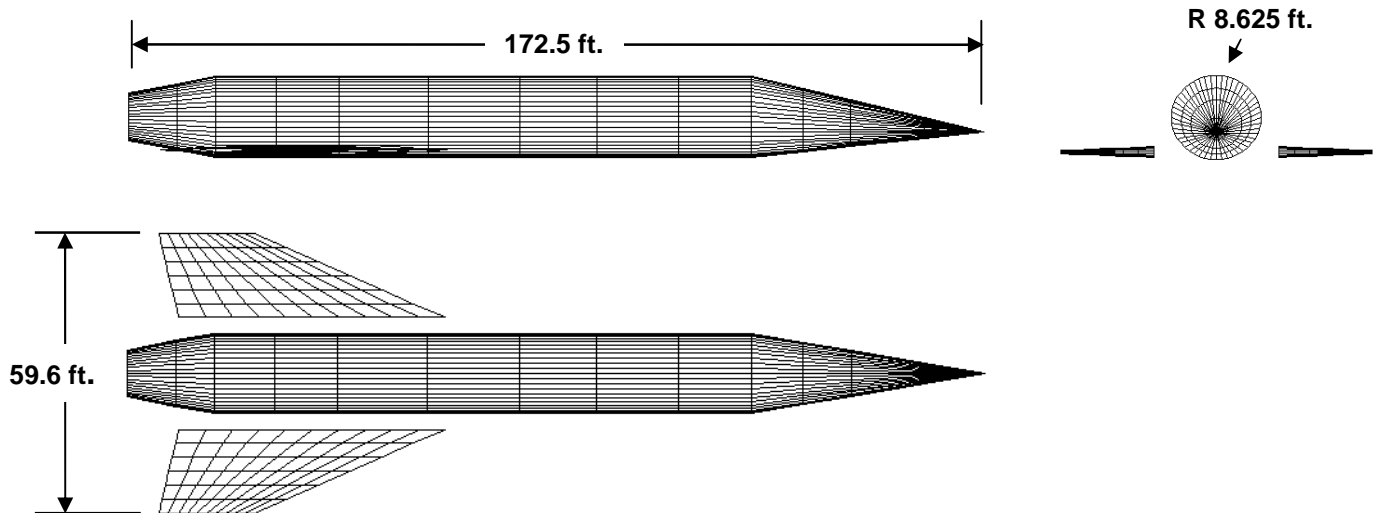


Figure 24: APAS Geometry for Argus RLV

The results of UDP and “wave drag” analysis on the Argus configuration are shown in Figure 25. The results are nearly identical to those from the Starsaber analysis. The drag increase above Mach 1.1 is more pronounced here, but drag seems to decrease again above Mach 1.5. Theoretical reference wing area for Argus is 2588.8 ft².

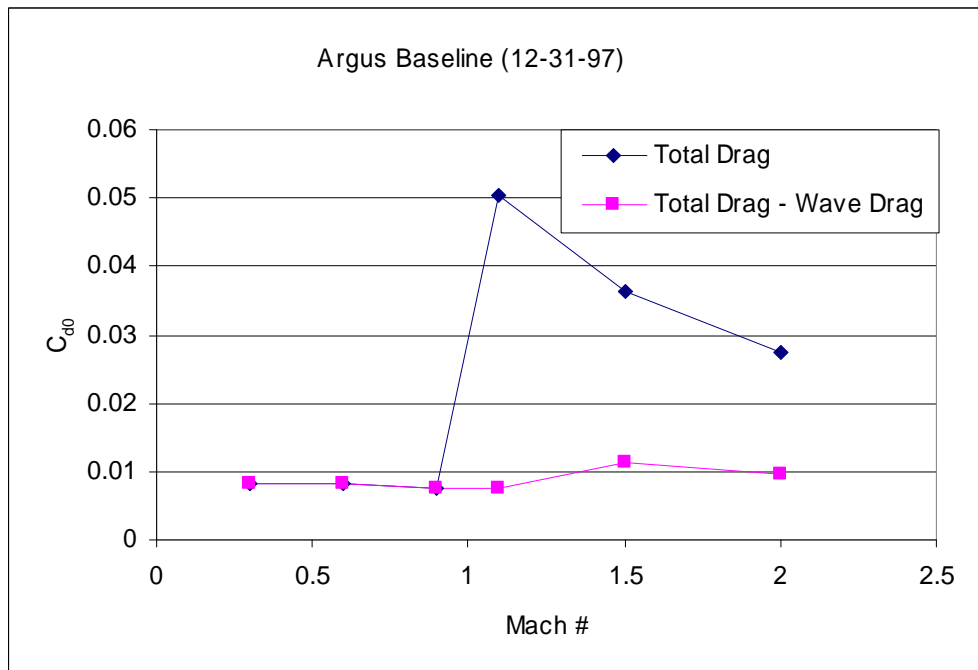


Figure 25. Argus APAS Results, With & Without Wave Drag

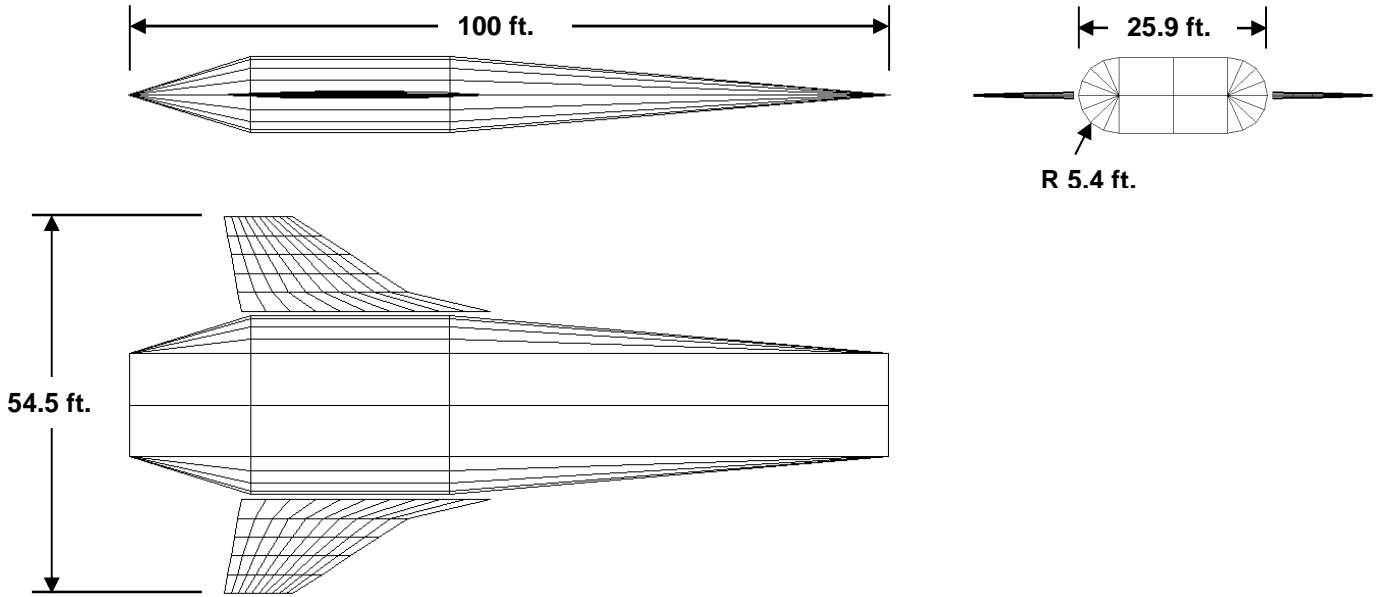


Figure 26. Stargazer APAS Results, With & Without Wave Drag

The final vehicle analysis was done on Stargazer, another RBCC powered RLV. The configuration of Stargazer, shown in Figure 26, is substantially different than that of any other geometry analyzed in this study. Transonic drag rise is again achieved through the addition of a wave drag term. The approximation works well because the last Mach number analyzed before wave drag terms are added is Mach 0.6. Drag appears to increase above Mach 1.5, but again further analysis is required to determine the cause. Theoretical reference wing area for Stargazer is 1440.3 ft².

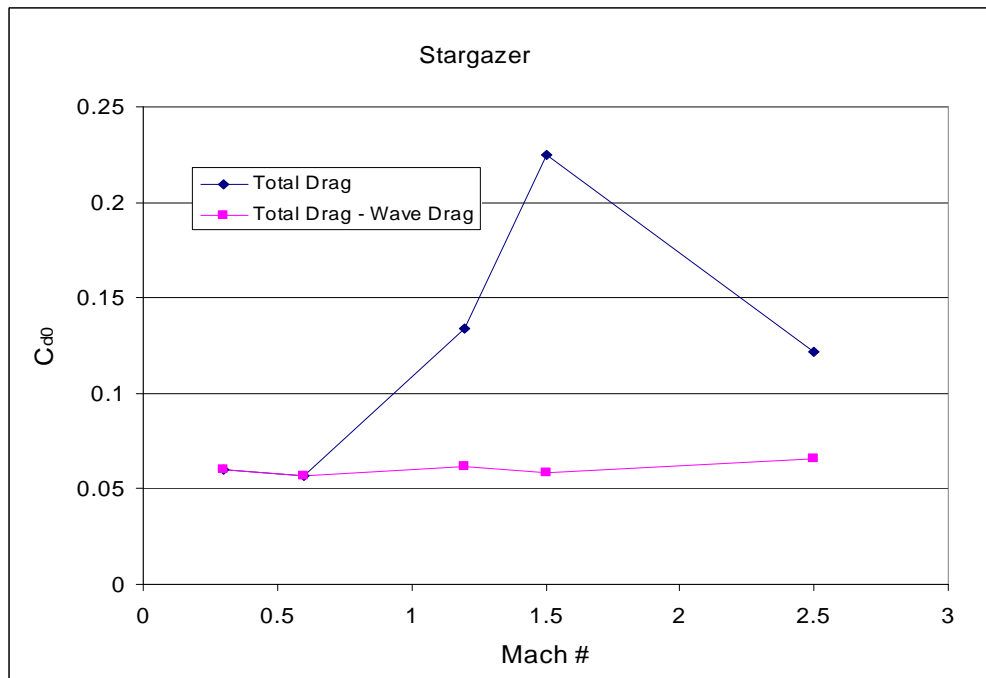


Figure 27. Stargazer APAS Results, With & Without Wave Drag

With the method by which APAS creates the transonic drag rise determined as the addition of wave drag above Mach 1, the next step was to check whether or not wave drag could be reduced by “coke-bottling” one of the trial configurations. Analysis of the original six configurations would then be repeated in another program, with the hopes of achieving results with which those from APAS could be measured and compared.

4.1.7 APAS “Coke-bottle” Geometry Results

The geometry of Trial 3 was modified by reducing the cross-sectional area of the fuselage in the region of the wing root as seen in Figure 28255 below.

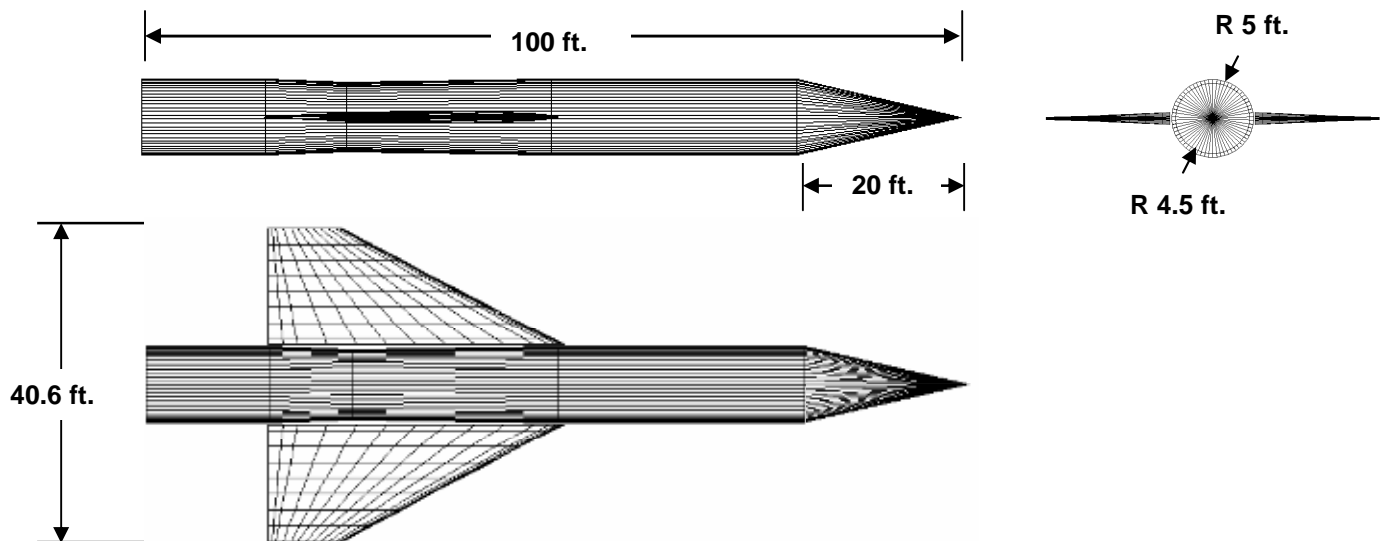


Figure 28. Trial 3b APAS Geometry

This modification results in a “coke-bottle” geometry that has been proven to reduce wave drag. The APAS results, when compared with those of the normal Trial 3 configuration, demonstrate that this method of reducing wave drag works in APAS. The “coke-bottle” geometry was analyzed only in APAS, in order to prove the validity of this method in the reduction of wave drag. The resulting area buildup can be found in Appendix B.

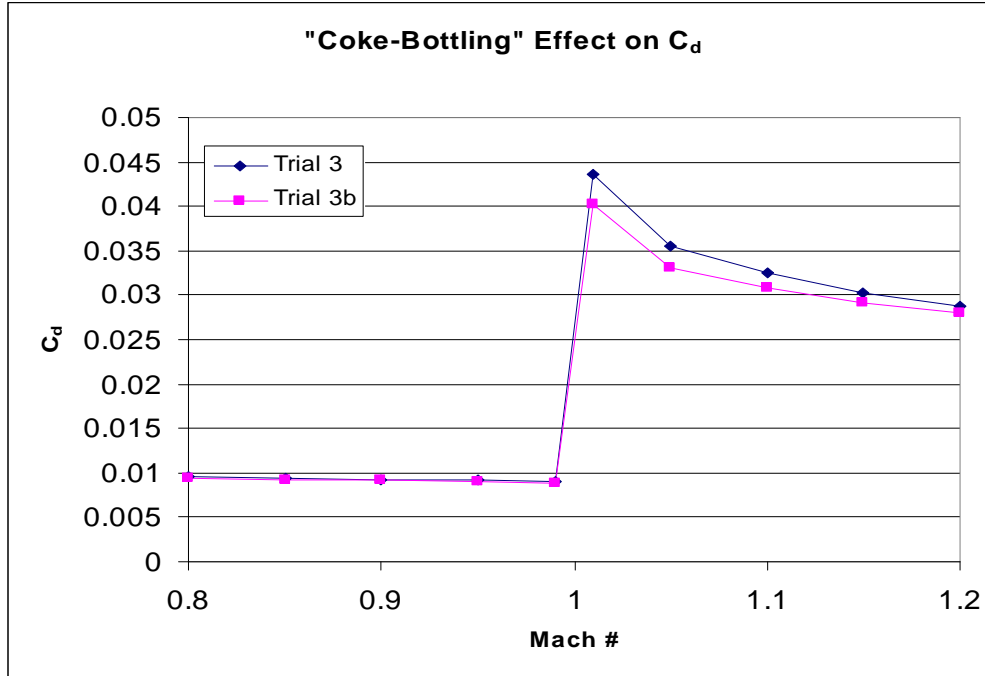


Figure 29. Trials 3 & 3b Total Drag APAS Results

Figure 29 shows the change in the total drag coefficient due to the “coke-bottle” modification. Drag is reduced only above Mach 1, where the wave drag term is added. The reduction in wave drag alone is shown in Figure 30, and is biggest at Mach numbers close to 1.

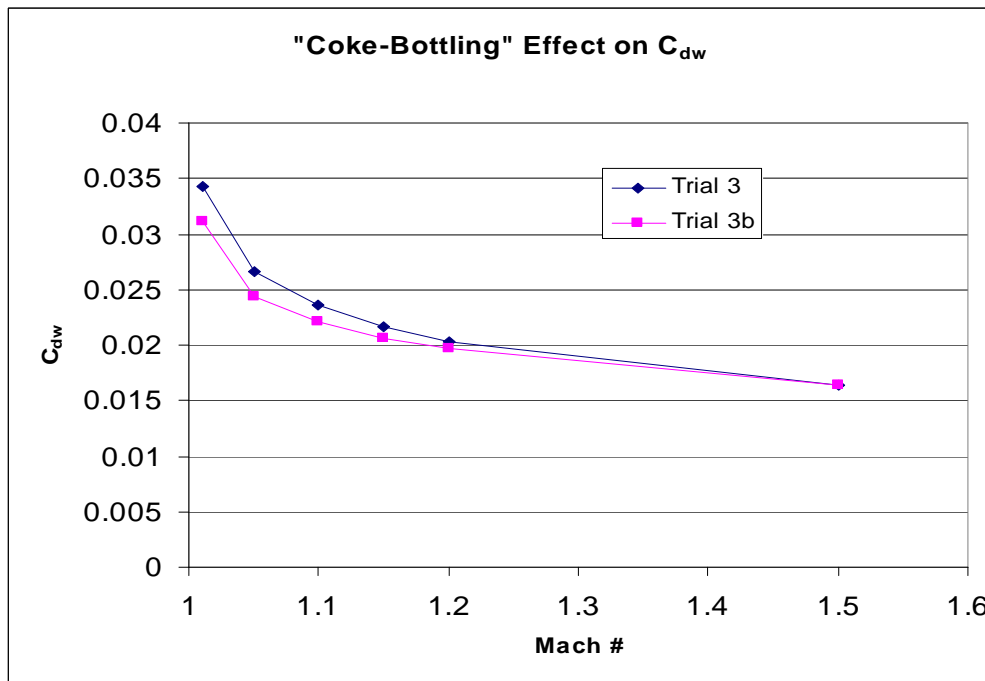


Figure 30. Trials 3 & 3b Wave Drag APAS Results

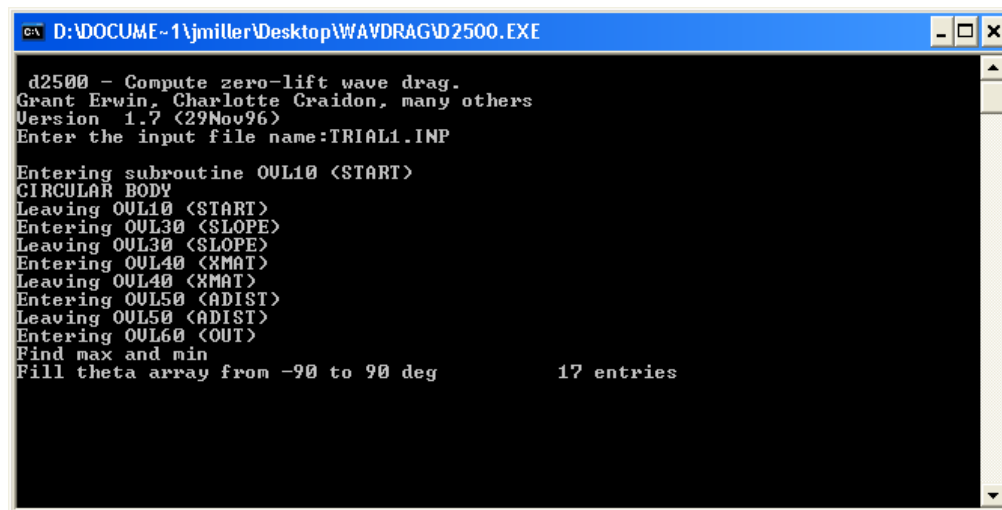
4.2 WAVDRAG

The program called WAVDRAG is also called NASA Langley Program 2500 – Wave Drag by Area Rule. The program is written in Fortran 77 and was developed in 1983. The program uses the numerical method developed by R.V. Harris as described in reference (9).

4.2.1 Program Description

Like the wave drag calculations in APAS, WAVDRAG's calculations are based on Whitcomb's area rule computation of equivalent bodies. Comparison of WAVDRAG zero-lift results with wave drag including lifting effects from APAS would help confirm the accuracy of APAS by checking the magnitude and trend of its results. A comparison would also possibly also provide evidence that the method used by APAS is actually based on those of WAVDRAG.

Unlike APAS, there is no graphic user interface for WAVDRAG. The user must follow a strict input file format in order to create a configuration that the program can analyze. The program has been modified to run in the command-prompt environment of Microsoft Windows. A screenshot of the program executing is shown in Figure 31.



```

c:\ D:\DOCUME~1\jmillr\Desktop\WAVDRAG\D2500.EXE
d2500 - Compute zero-lift wave drag.
Grant Erwin, Charlotte Craidon, many others
Version 1.7 (29Nov96)
Enter the input file name:TRIAL1.INP
Entering subroutine OUL10 (START)
CIRCULAR BODY
Leaving OUL10 (START)
Entering OUL30 (SLOPE)
Leaving OUL30 (SLOPE)
Entering OUL40 (XMAT)
Leaving OUL40 (XMAT)
Entering OUL50 (ADIST)
Leaving OUL50 (ADIST)
Entering OUL60 (OUT)
Find max and min
Fill theta array from -90 to 90 deg          17 entries

```

Figure 31: WAVDRAG Command Screen

4.2.2 Geometry Input Procedure

A detailed explanation of the geometry input requirements is given in Appendix A, along with the WAVDRAG input files for the six trial configurations previously analyzed in APAS. The input structure is somewhat similar to that of APAS's. Fuselages are input as combination of body-axis coordinates and areas (assuming a circular fuselage). Geometries that are more complicated are created using a three-dimensional coordinate system to specify the body shape at each body-axis location. Wings are defined as sets of airfoils joined by surfaces. The wings analyzed for this study were input using two airfoils, one at the wing root and one at the wing tip. Airfoil shape coordinates for each wing-body configuration were obtained directly from each trial's respective APAS model. An example of the APAS "edit" screen displaying airfoil shape coordinates is shown in Figure 32, which displays the root airfoil of wing 1 attached to fuselage 1.

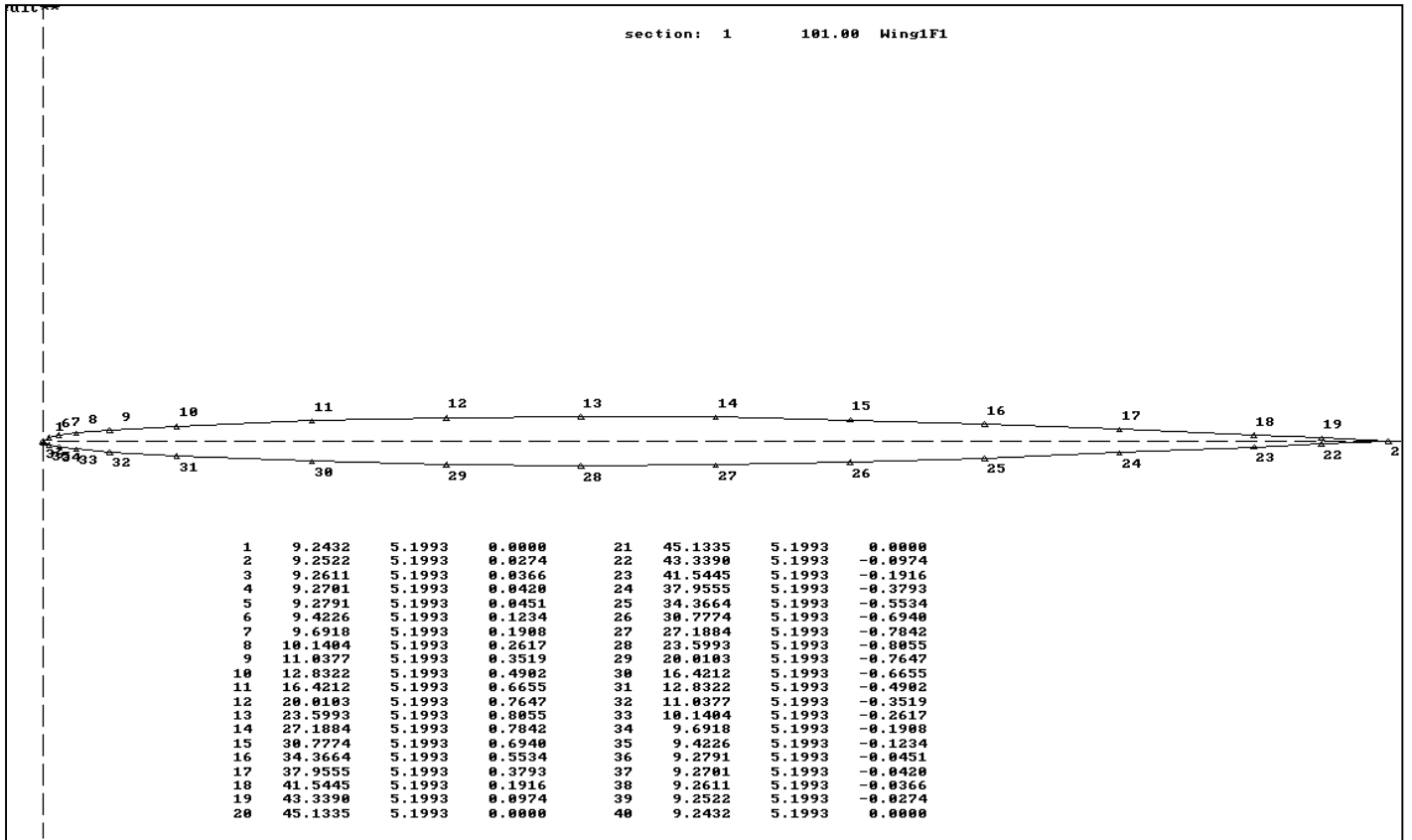


Figure 32. Root Airfoil of Trial 3 Configuration

4.2.3 Computation Procedure and Results

WAVDRAG is executed by typing the input file name at the command prompt. The program creates the specified number of equivalent bodies and calculates the integrated average of the wave drag results to obtain the configuration's wave drag. Table 2 shows the total D/q at all 17 cutting angles of each configuration analyzed.

θ (degrees)	Total D/Q					
	Trial 1	Trial 2	Trial 3	Trial 4	Trial 5	Trial 6
-90	18.903389	2.952193	22.482616	21.208817	7.396546	7.393107
-78.75	18.905067	2.952292	22.454659	21.198866	7.37816	7.36924
-67.5	18.902529	2.952283	22.397957	21.162766	7.333117	7.326739
-56.25	18.905151	2.952292	22.341856	21.120119	7.282824	7.284153
-45	18.903313	2.952202	22.289091	21.076923	7.249099	7.247213
-33.75	18.905071	2.952293	22.246429	21.046988	7.230801	7.218808
-22.5	18.902534	2.952245	22.213982	21.022324	7.222719	7.202837
-11.25	18.904808	2.952292	22.198305	21.011692	7.219873	7.195025
0	18.903433	2.952148	22.190899	21.006002	7.218596	7.192527
11.25	18.904808	2.952292	22.198305	21.011692	7.219873	7.195025
22.5	18.902534	2.952245	22.213982	21.022324	7.222719	7.202837
33.75	18.905071	2.952293	22.246429	21.046988	7.230801	7.218808
45	18.903313	2.952202	22.289091	21.076923	7.249099	7.247213
56.25	18.905151	2.952292	22.341856	21.120119	7.282824	7.284153
67.5	18.902529	2.952283	22.397957	21.162766	7.333117	7.326739
78.75	18.905067	2.952292	22.454659	21.198866	7.37816	7.36924
90	18.903389	2.952193	22.482616	21.208817	7.396546	7.393107

Table 2. WAVDRAG D/Q Results at 17 Cutting Angles

The configuration with the highest wave drag is the configuration with the greatest cross sectional area. Trial 3 consists of the larger wing mated to the larger fuselage. The rest of the results also follow expectations.

5.0 APAS and WAVDRAG Comparisons

The results of the two programs are compared in two ways. Both programs generate area build-up plots used to find the shape of equivalent bodies of revolution. Both programs also output a wave drag coefficient (C_{Dw}) at each Mach number.

5.1 Area Comparisons

APAS displays all of the results for each wave drag calculation at a given Mach number at once. The area build-up, along with D/q at each cutting angle, are output as a graphic for each Mach number as shown in Figure 33. Rather than display five such figures for each configuration, one for each Mach number over 1, a representative figure for each trial will be shown at a Mach number of 1.01. The lines along the bottom of the APAS graphic are a legend generated by APAS, not part of the results. Area build-ups are given for cutting angles of 90, 45, 0, -45, and -90 degrees. The build-up at each of these cutting angles can be examined by matching the pattern given at the bottom to the identical pattern in the graph. The x-axis in these graphs represents location on the body-axis, beginning at the tip of the vehicle's nose. The y-axis gives the total cross-sectional area at the specified cutting angle.

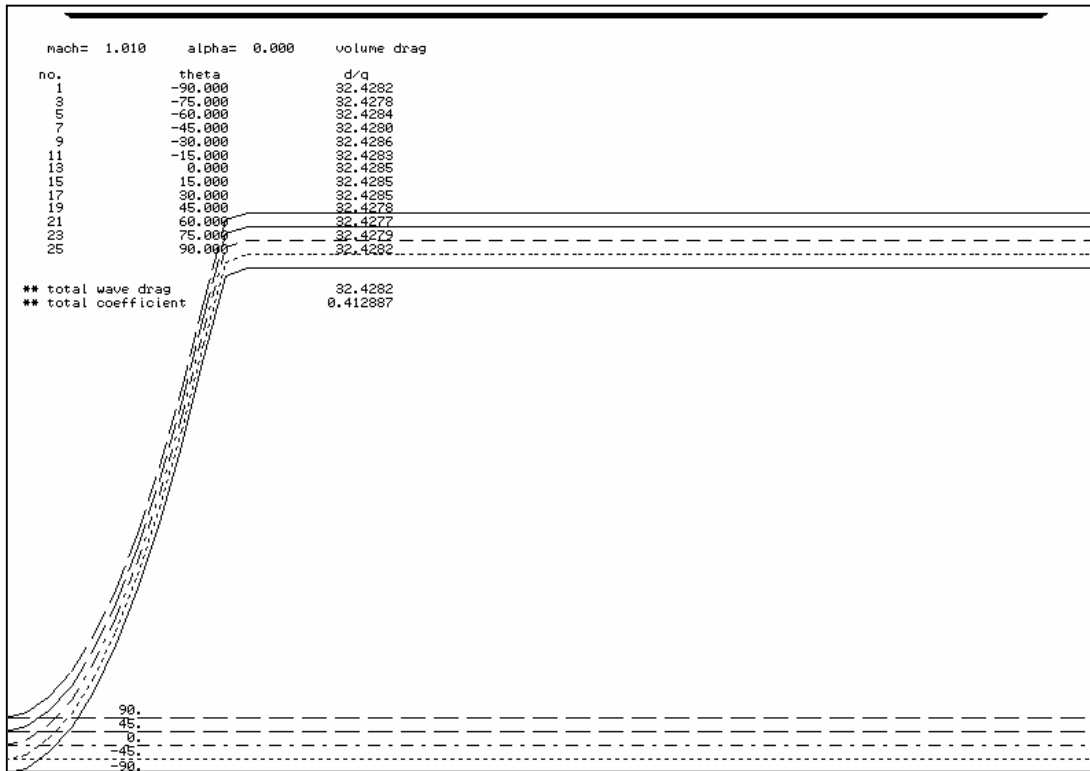


Figure 33: APAS Area Build-up for Trial 1

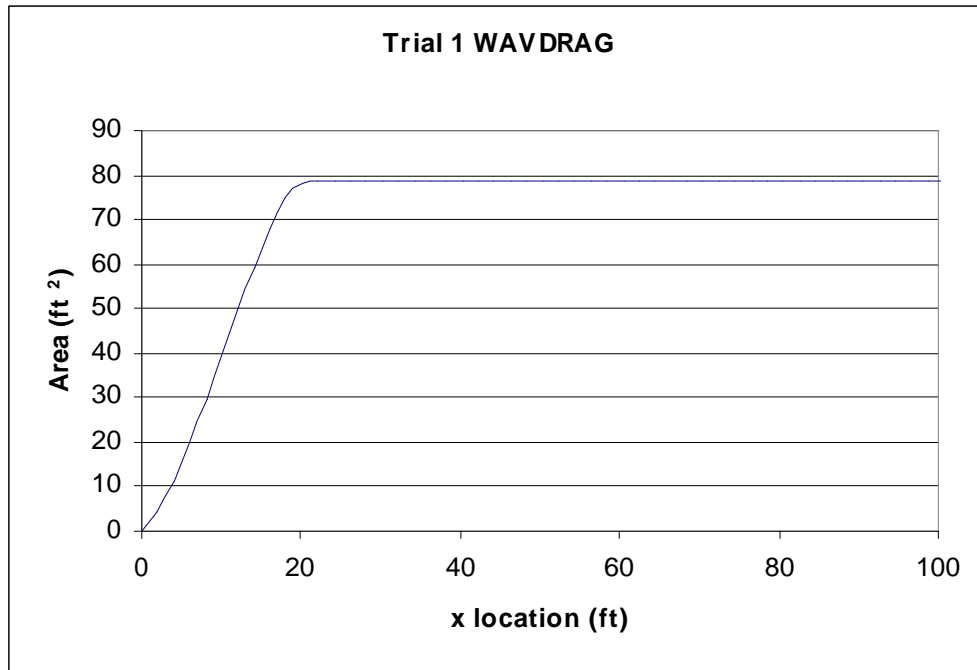


Figure 34. WAVDRAG Area Build-up for Trial 1

The shape of the area build-up for the trial 1 configuration in WAVDRAG is shown in Figure 34. WAVDRAG outputs the area build-up as the average of that of the areas obtained from the cutting planes at each roll angle θ . The curve is of the same shape as the APAS build-up, which demonstrates that the two programs are analyzing the same configuration and are generating similar, if not identical, sets of equivalent bodies. The maximum area reached in the WAVDRAG figure is that of a circle with a radius of 5 ft, which is the maximum cross-sectional area of trial 1.

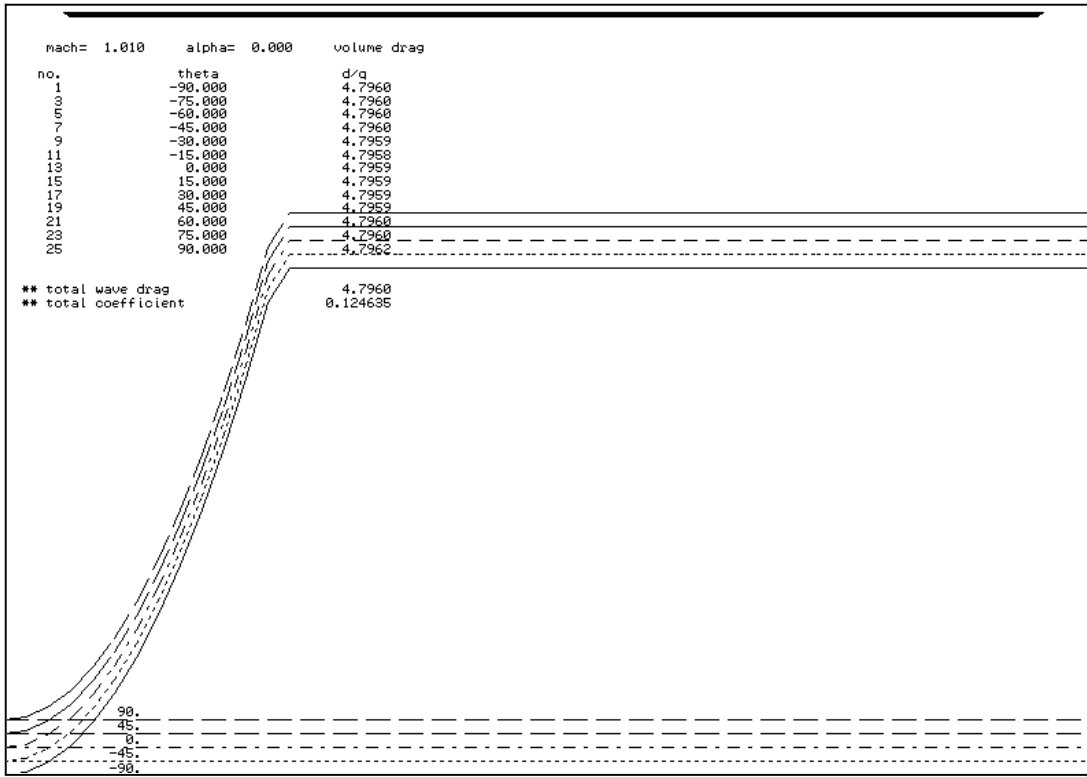


Figure 35. APAS Area Build-up for Trial 2

The area build-ups for trial 2 from APAS and WAVDRAG are shown in Figures 35 and 36 respectively. Their shapes agree again, and the magnitude of the area as shown in the WAVDRAG graph corresponds to the area of a circle with radius 3.5 ft.

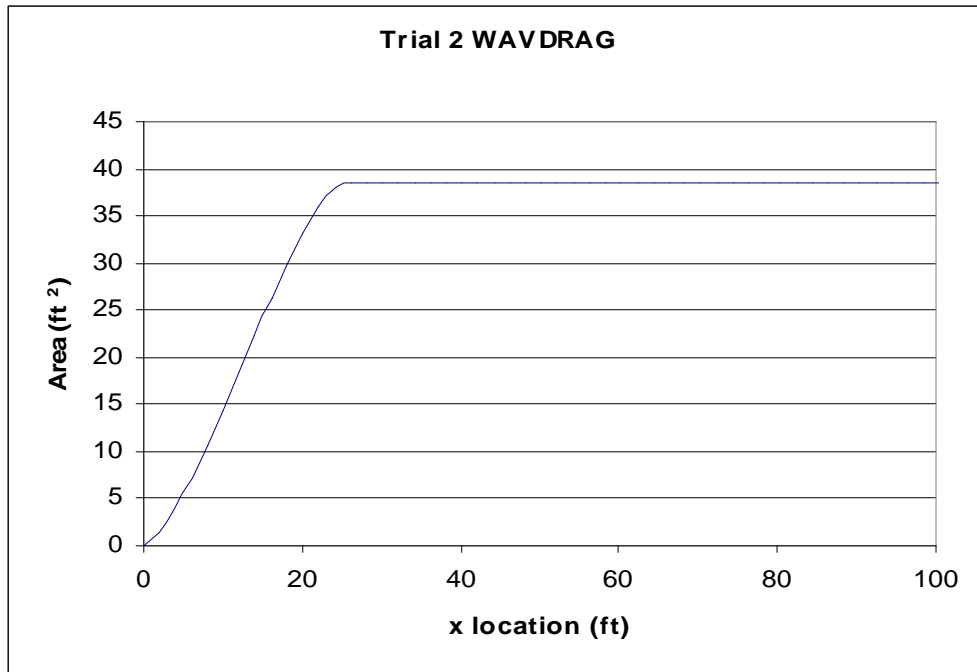


Figure 36. WAVDRAG Area Build-up for Trial 2

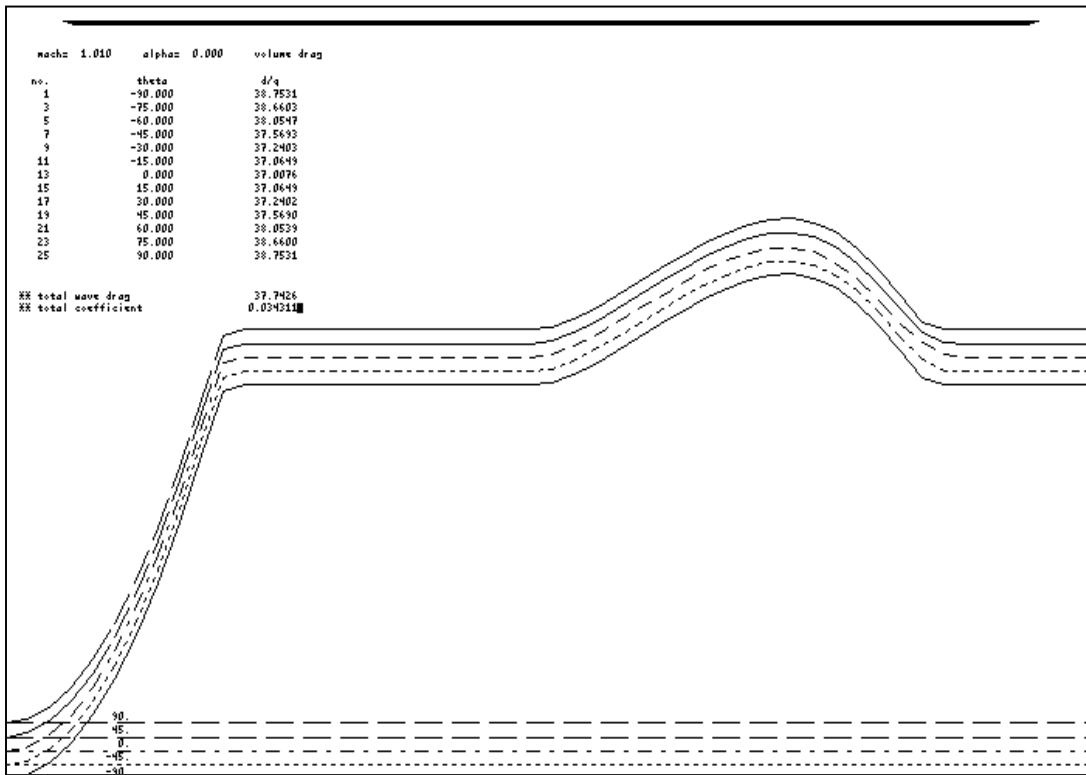


Figure 37. APAS Area Build-up for Trial 3

Figures 37 and 38 show the area build-up for the first wing-body configuration analyzed, trial 3. The area build-up is identical to that of trial 1, with the addition of a local area rise between 55 and 80 feet due to the wing.

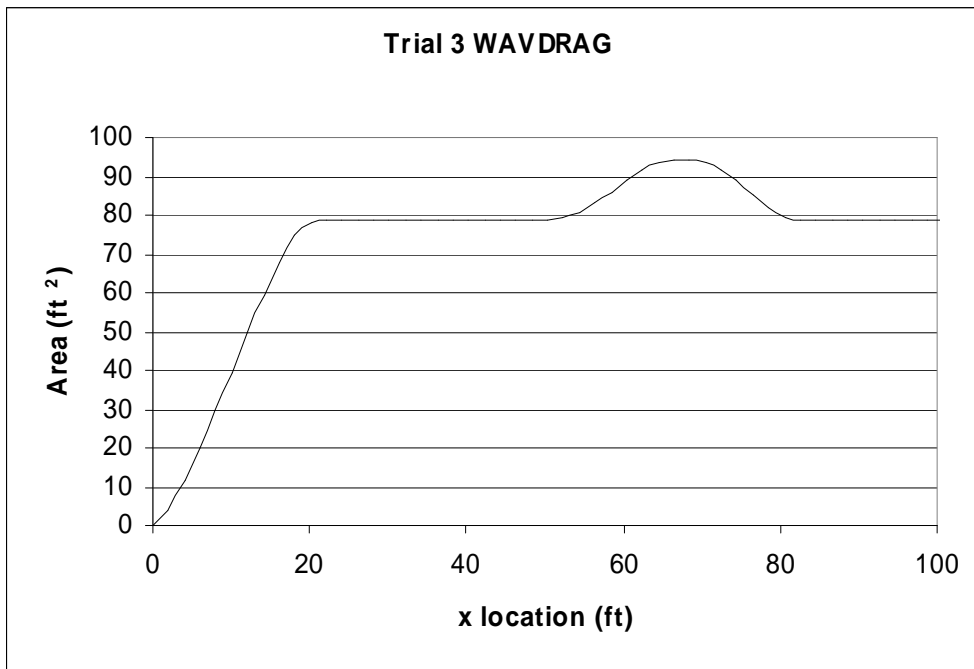


Figure 38. WAVDRAG Area Build-up for Trial 3

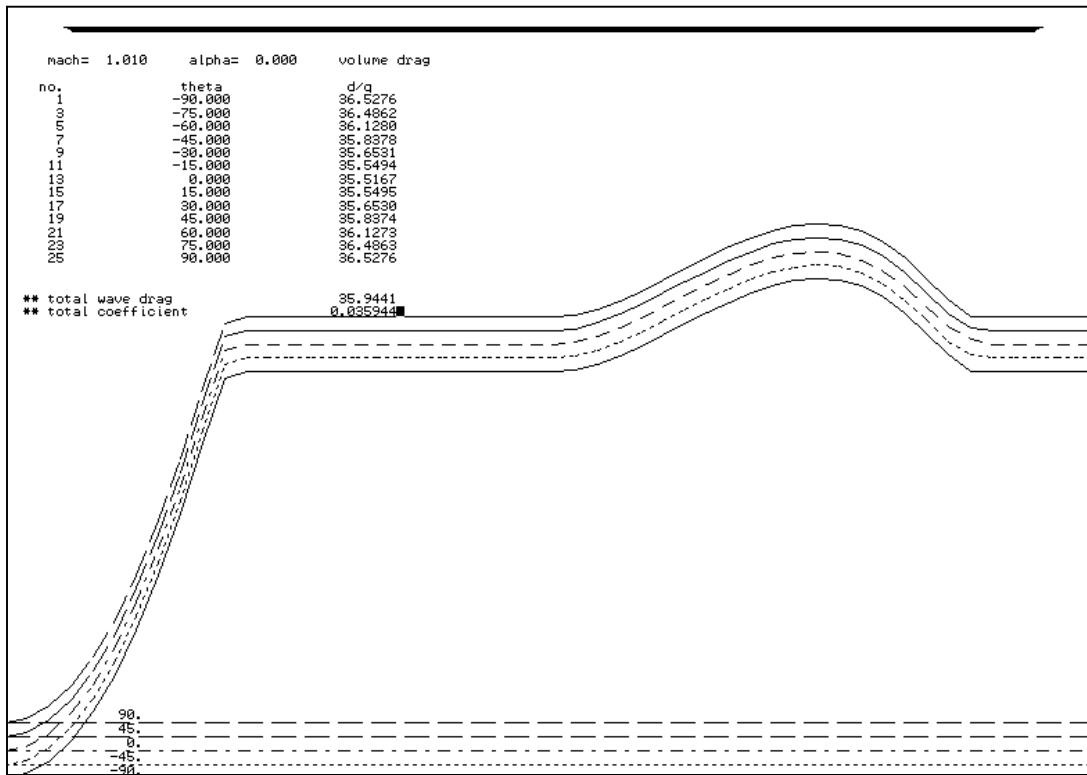


Figure 39. APAS Area Build-up for Trial 4

The area build-up graphs for trial 4, Figures 39 and 40, both show the same initial shape as the build-ups of trial 1. The local area increase in the trial 4 graphs is slightly smaller due to the lesser wing area of wing 2.

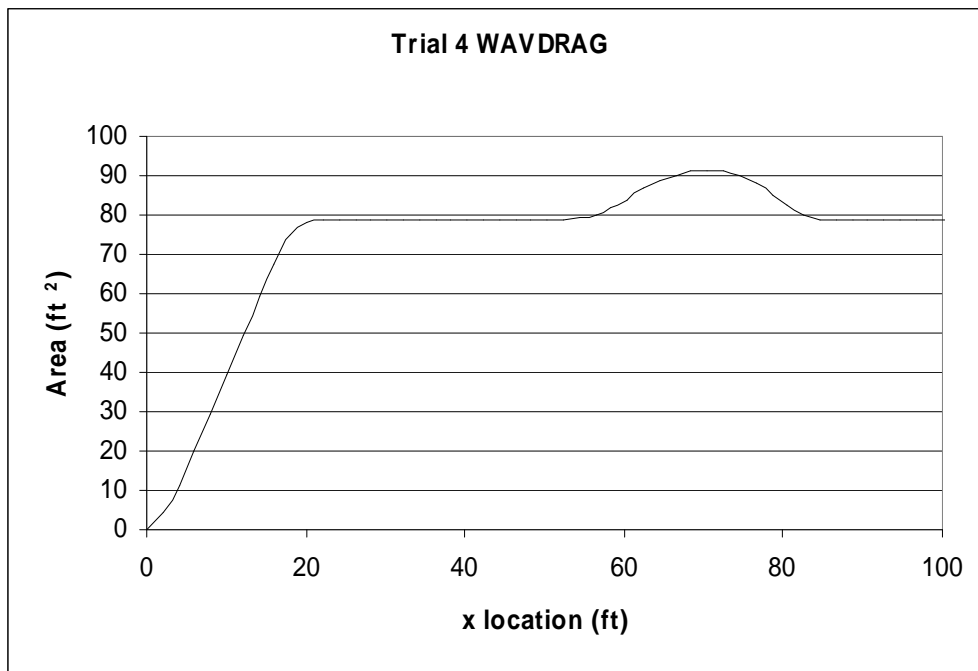


Figure 40. WAVDRAG Area Build-up for Trial 4

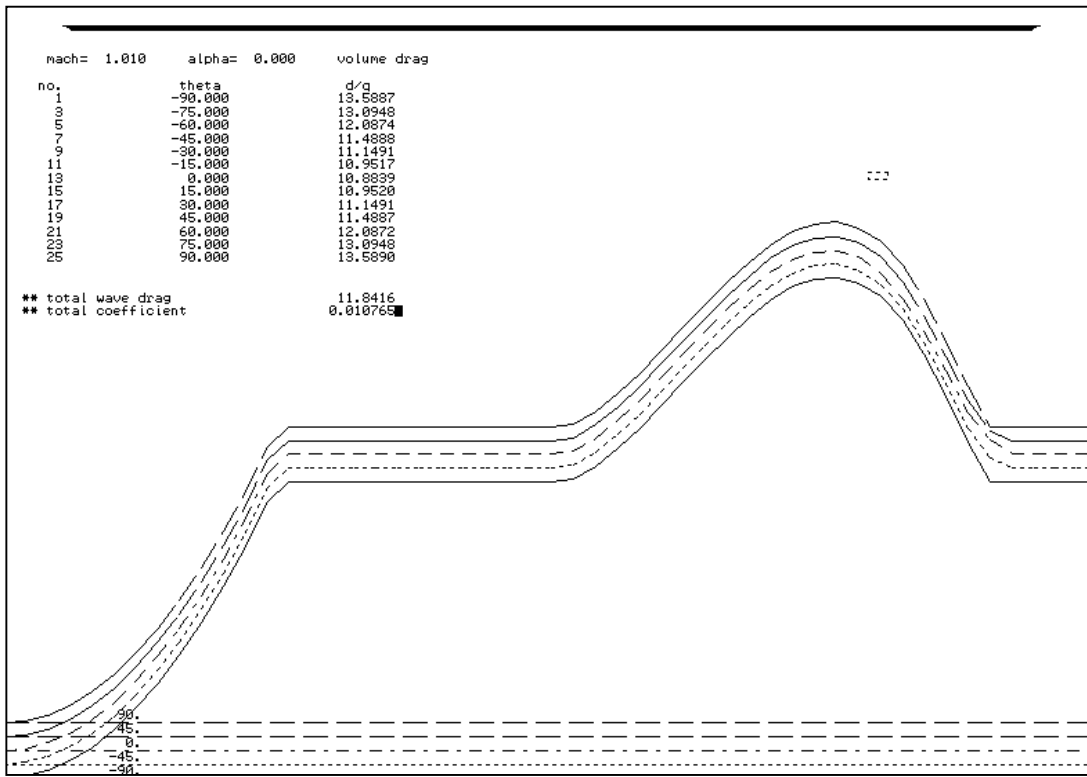


Figure 41. APAS Area Build-up for Trial 5

Figures 41 and 42 show the change in shape of the area build-up in the first trial combining the smaller fuselage with a wing. The local area rise due to the wing is much more pronounced on the smaller fuselage.

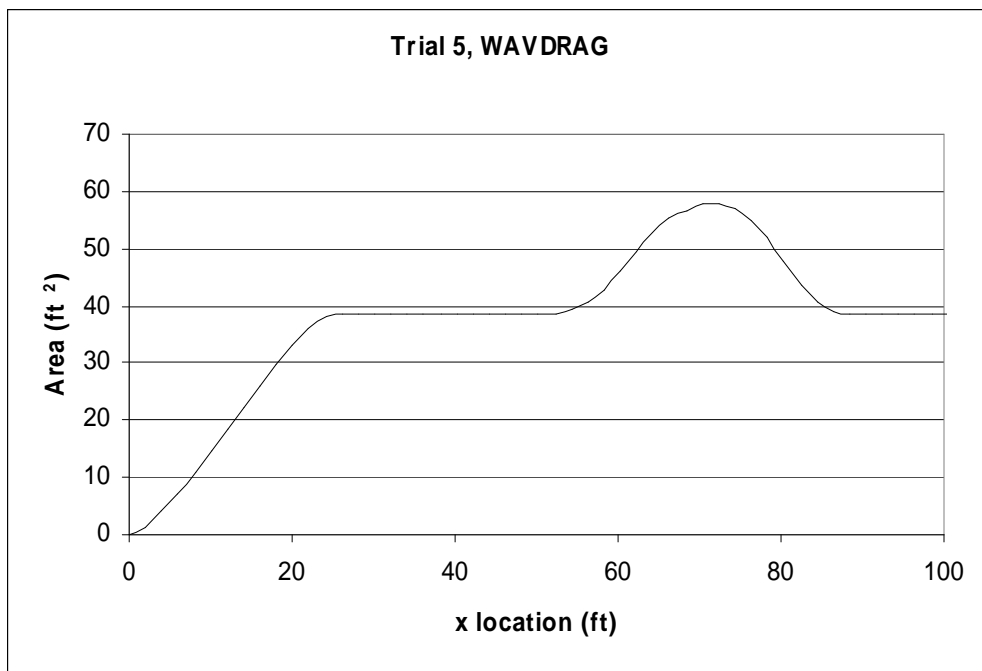


Figure 42. WAVDRAG Area Build-up for Trial 5

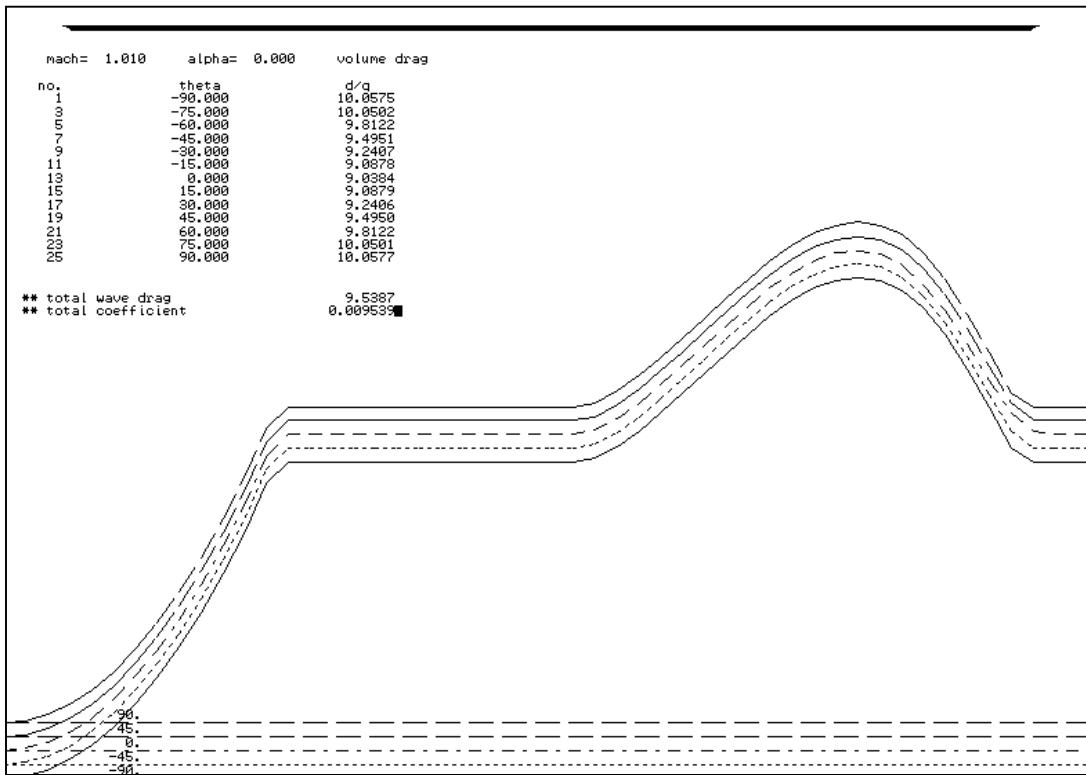


Figure 43. APAS Area Build-up for Trial 6

The area build-ups of the final configuration are shown in Figures 43 and 44. The smaller wing produces a less drastic local area rise than in the previous trial with the larger wing. The shapes of the graphs from APAS and WAVDRAG once again coincide.

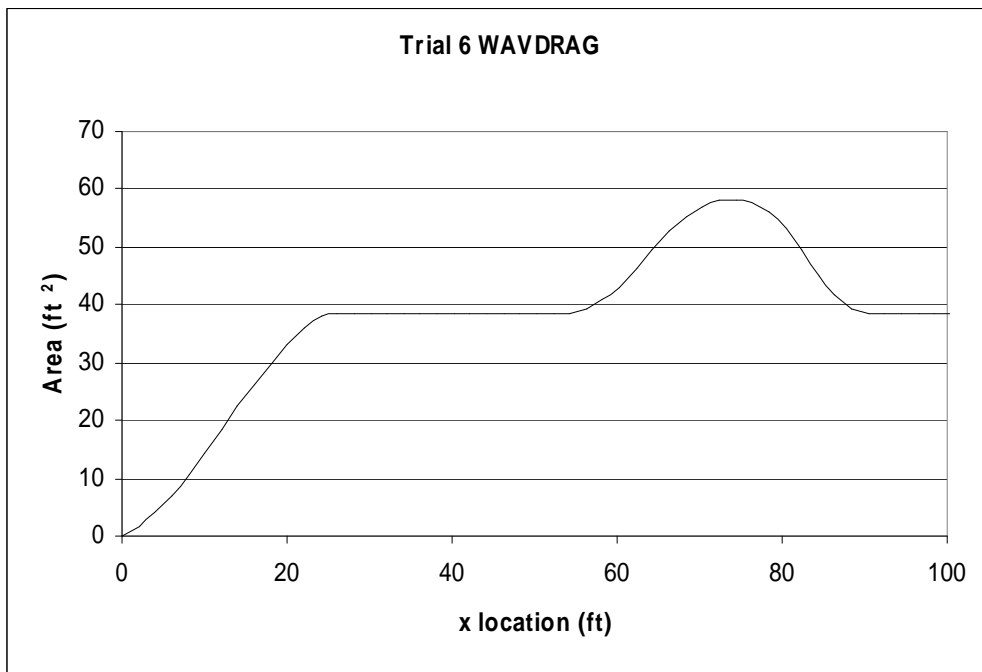


Figure 44. WAVDRAG Area Build-up for Trial 6

Area build-up graphs were also generated for the wave drag analyses of the 3 RLV configurations. These configurations were not run in WAVDRAG, so no comparison was made with the APAS results. The APAS build-ups can be found in Appendix B of this report.

5.2 Wave Drag Comparisons

The second and more conclusive comparison between APAS and WAVDRAG is that of the actual wave drag coefficients of each trial configuration generated by the two programs. Figure 45 shows the wave drag calculated by the wave subprogram of APAS and the results of the WAVDRAG analysis of the trial 1 configuration. Unlike APAS, WAVDRAG will generate results at Mach 1, but no lower.

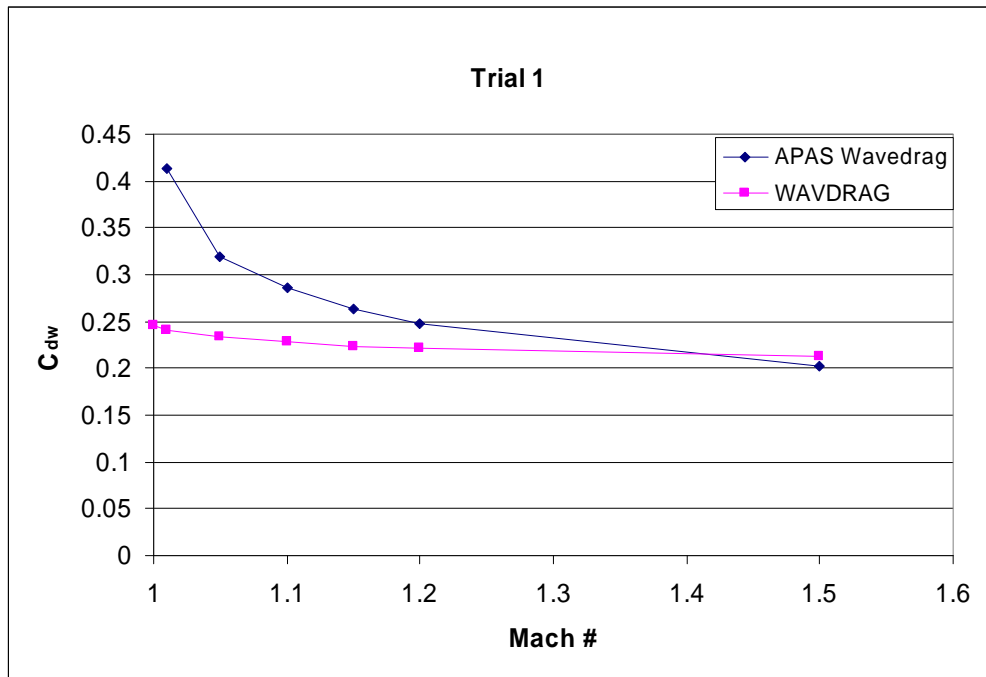


Figure 45. Trial 1 Wave Drag Comparison

WAVDRAG predicts a wave drag coefficient forty percent lower than APAS at Mach 1.01 due to the difference in the ways the programs calculate wave drag, one as zero-lift wave drag and the other as wave drag that includes that due to lift. The plots

converge on each other as Mach number increases, and cross just above Mach 1.4. The Mach number range analyzed for these comparisons was extended to Mach 1.5 in order to determine at what point the programs agreed.

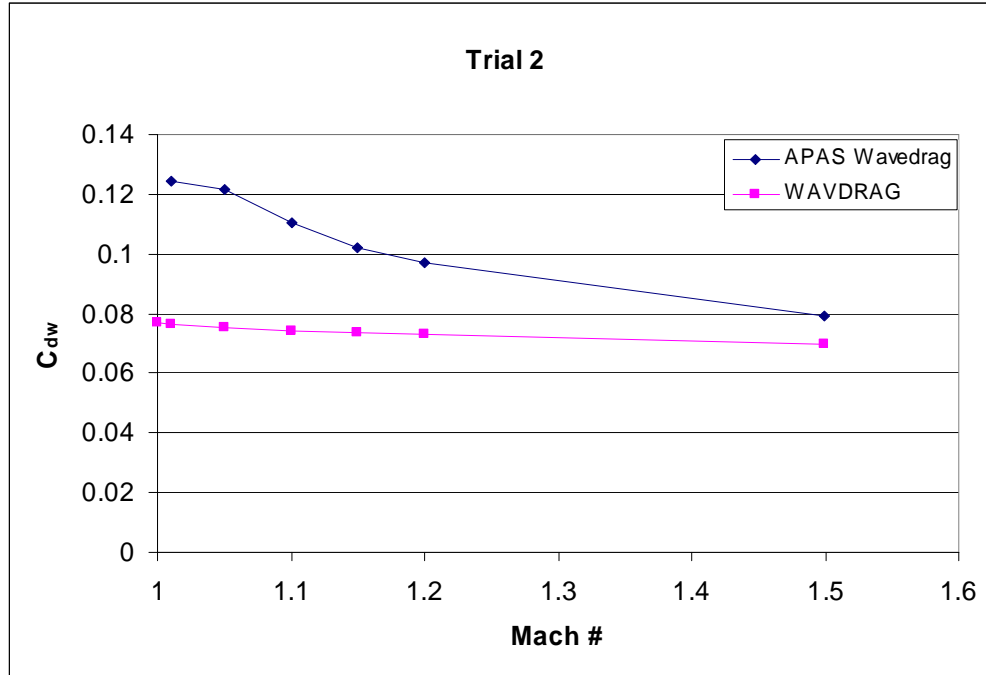


Figure 46. Trial 2 Wave Drag Comparison

Figure 46 shows the wave drag comparison for the second configuration. The wave drag coefficients of the two programs have not yet converged by Mach 1.5, but appear to converge somewhere around Mach 1.7. The trend appears to be the same, but APAS again predicts much higher values immediately after Mach 1.

The results for trial 3, Figure 47, are similar to those for trial 1. The coefficients of the two programs meet around Mach 1.4, but then appear to diverge again. APAS predicts higher wave drag close to Mach 1, and lower wave drag as Mach number increase past 1.4. In the wing-body trials, differences in the results can certainly be attributed to wave drag due to lift including in APAS' results.

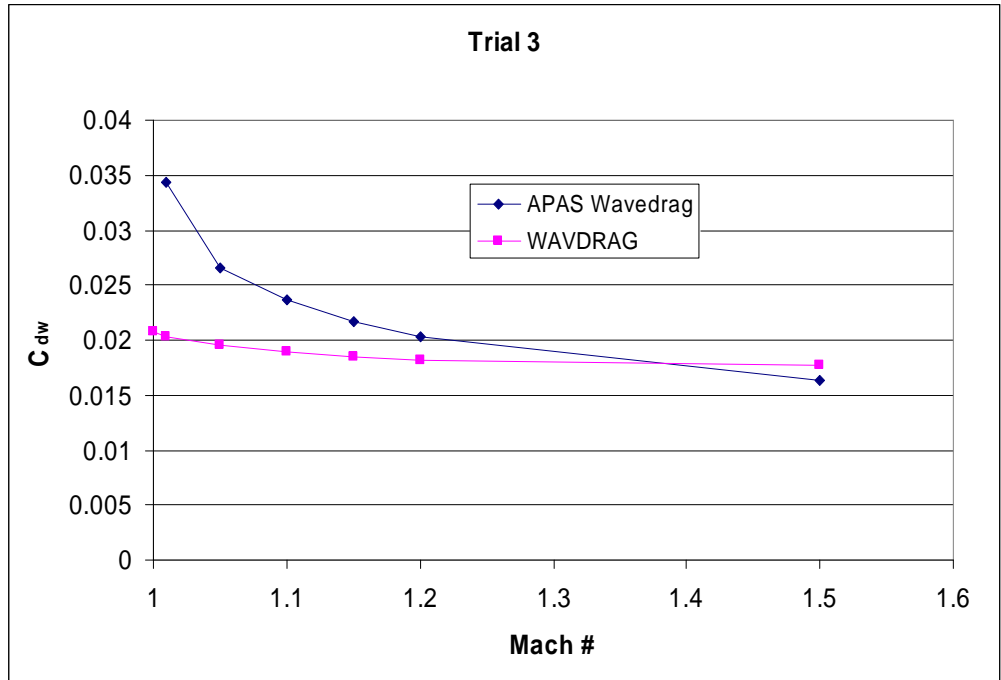


Figure 47. Trial 3 Wave Drag Comparison

The comparison results for the first second wing-body combination can be seen in Figures 48. The results follow the same trend as results from the previous trials.

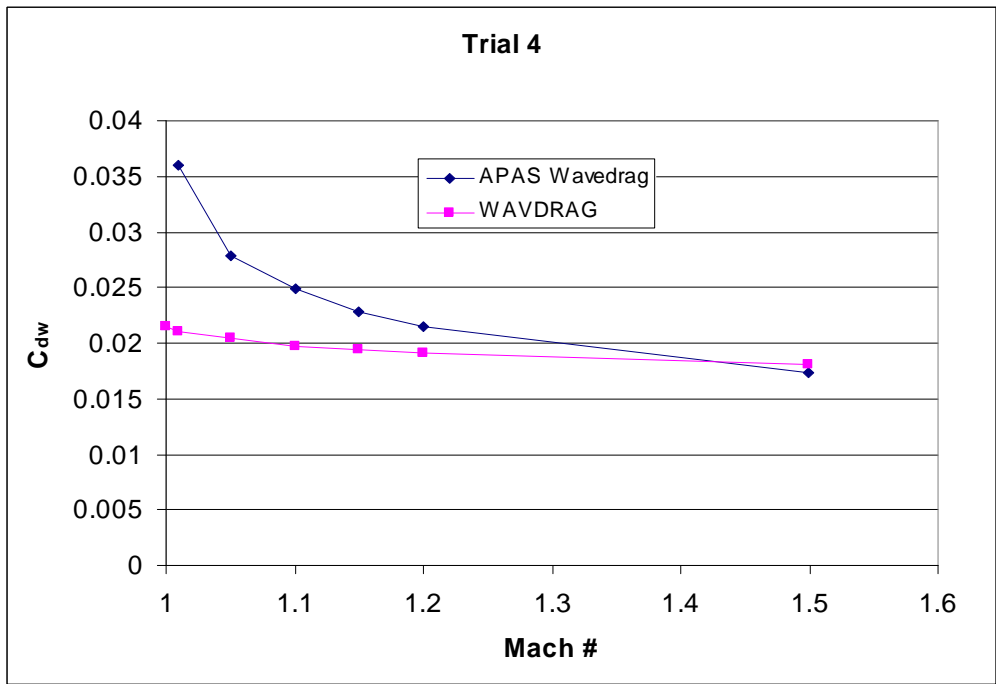


Figure 48. Trial 4 Wave Drag Comparison

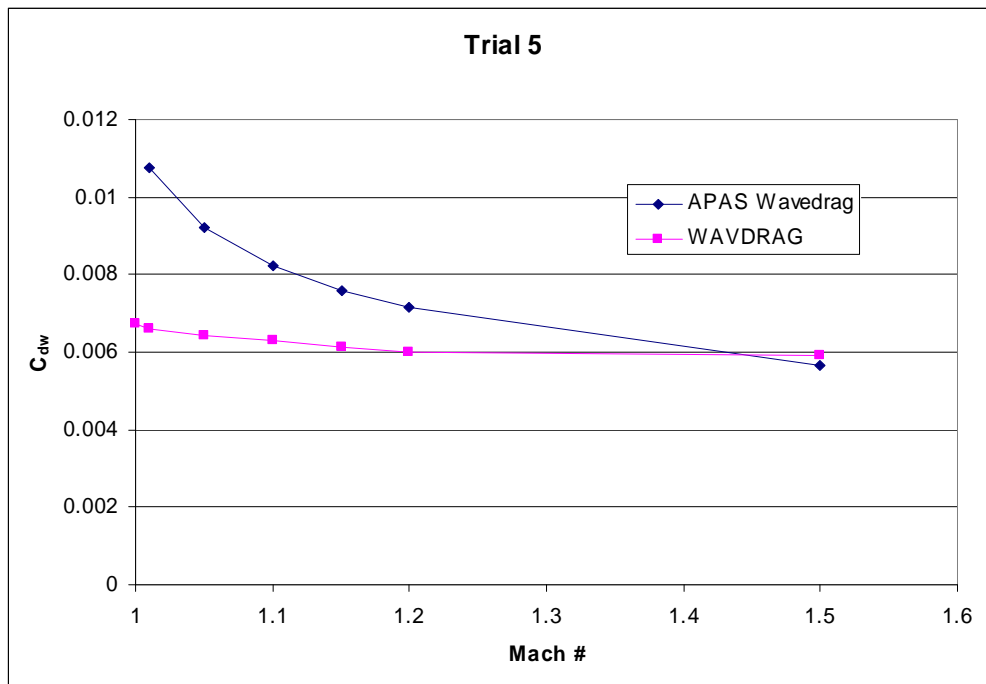


Figure 49. Trial 5 Wave Drag Comparison

The wave drag comparison for the last two trials are shown in Figures 49 and 50. The effect the different wing geometries have on the wave drag coefficients is more pronounced here, but the trend of APAS predicting higher initial values and lower high Mach number wave drag coefficients due to its more inclusive calculation continues.

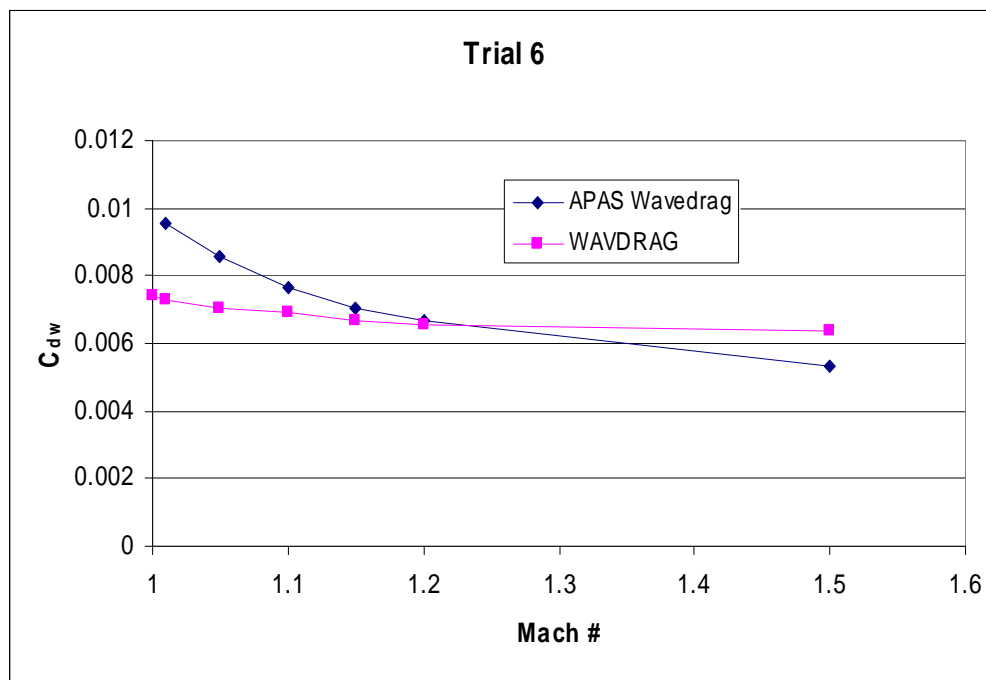


Figure 50. Trial 6 Wave Drag Comparison

The final comparison results, Figures 51 and 52, show the complete results from each program. Comparison of the two figures shows that APAS and WAVDRAG agree on the relative magnitudes of the wave drag coefficients of the six trial configurations.

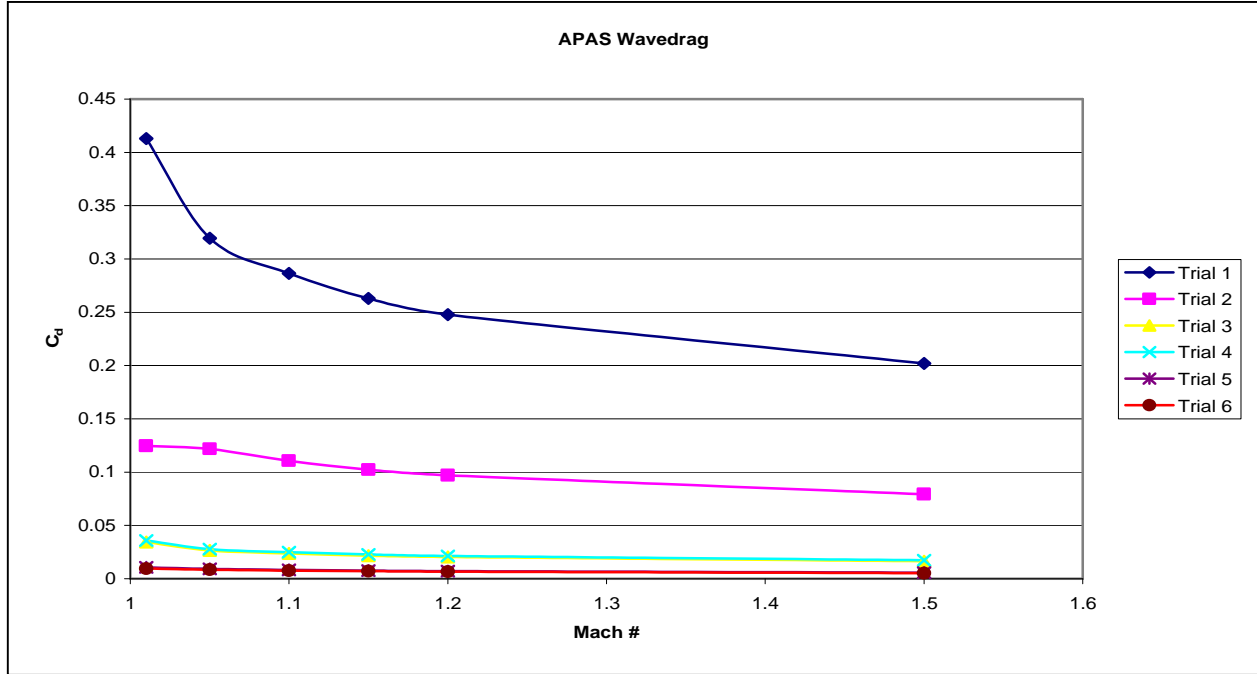


Figure 51. Summary of APAS Wave Drag Results

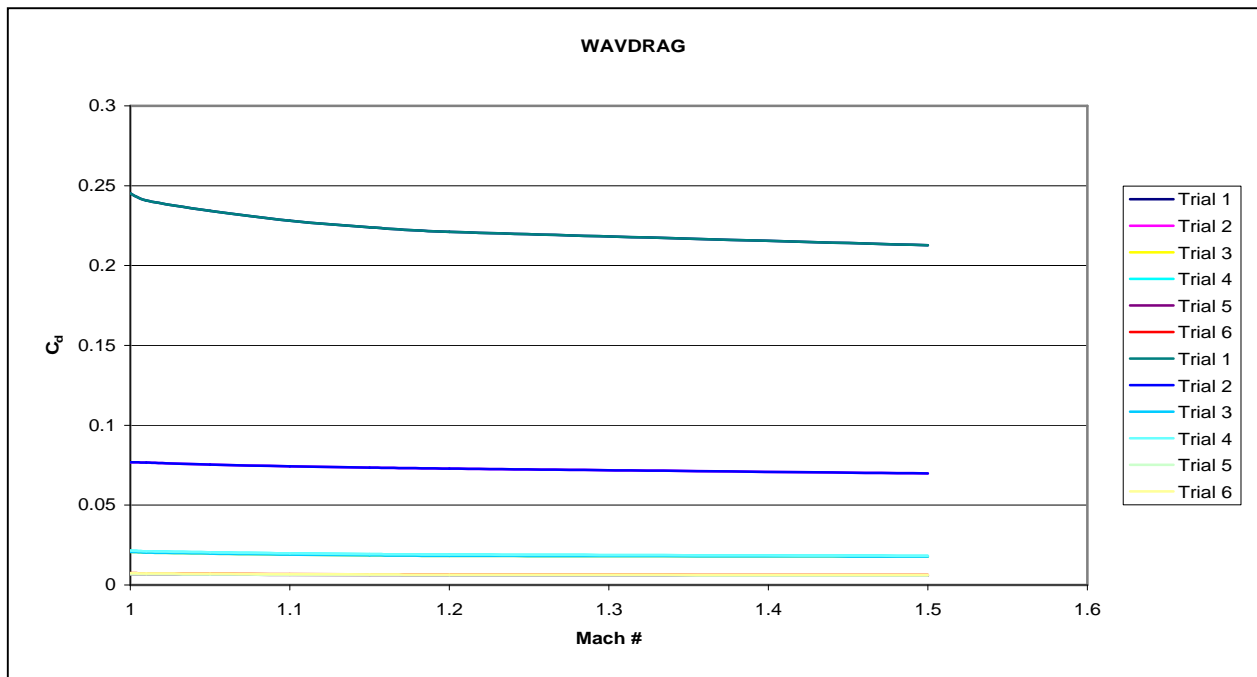


Figure 52. Summary of WAVDRAG Wave Drag Results

6.0 Conclusions

It has been shown that APAS uses the addition of a wave drag coefficient to the total drag coefficient at speeds greater than Mach 1 in order to achieve a transonic drag rise. This approximation works provided the user is aware of this and can schedule the last run before Mach 1 at a Mach number such that interpolating yields acceptable transonic drag rise. The method by which APAS makes these calculations is a version of Richard Whitcomb's linear area rule, the same method used by NASA Langley's WAVDRAG program. The calculations in APAS also appear to be an evolution of those in WAVDRAG. The two programs calculate their respective types of wave drag in a similar manner, lending credibility to the results of each other. APAS consistently predicts higher wave drag coefficients at Mach numbers immediately following 1, due to the differences in its calculation methods as compared to WAVDRAG .

APAS could be modified to use the nonlinear area rule which is capable of predicted transonic drag below Mach 1. Such a modification would require an individual with a working knowledge of the APAS source code as well as the nonlinear area rule, and would likely not be a trivial task. The approximation APAS uses is no doubt acceptable to most users who rely on APAS as a first glance aerodynamic analysis tool useful for conceptual design. More in-depth analysis would be required in the preliminary stages of design.

7.0 Acknowledgments

I would first like to thank Dr. John Olds of the Georgia Institute of Technology for his guidance on this project. James McIntire, a full time employee of the Lincoln Laboratory in Boston, taught me how to use APAS and has always been eager to help as both coworker and a friend. For that I would like to thank him as well.

The WAVDRAG analysis would not have been possible without the assistance of Ralph Carmichael, who oversees distribution of the PDAS (Public Domain Aeronautical Software) CD-ROM on which I found the program and pointed me towards a local copy, saving me both time and \$295. Without the instructional information he added to the program, learning how to use WAVDRAG would have been substantially more difficult. I would also like to thank Mark Waters of Georgia Tech's Aerospace Systems Design Lab for providing me with the actual copy of PDAS that I used.

8.0 References

¹Guynn, M.D., "Aerodynamic Preliminary Analysis System, Beginner's Guide," NASA Langley Research Center.

²Carmichael, R., "README for NASA Langley Program D2500: Wave Drag by Area Rule," PDAS CD-ROM, 2001.

³Harris, R.V., Jr., "An Analysis and Correlation of Aircraft Wave Drag," NASA TMX 947, 1964.

⁴Jones, R.T., "Theory of Wing-Body Drag at Supersonic Speeds," NACA 1284, 1963.

⁵Malmuth, N., Wu, C.C., and Cole, J.D., "Transonic Drag Estimation and Optimization Using the Nonlinear Area Rule," AIAA 86-1798, 1986.

⁶Bonner, E., Clever, W., and Dunn, K., "Aerodynamic Preliminary Analysis System II, Part I - Theory," NASA Contractor Report 182076, 1991.

⁷Whitcomb, R.T., "A Study of the Zero-Lift Drag-Rise Characteristics of Wing-Body Combinations Near the Speed of Sound." NACA 1273, 1952.

⁸Jones, R.T., "Minimum Wave Drag for Arbitrary Arrangements of Wings and Bodies," NACA TN 3530, 1955.

⁹Harris, R.V., Jr., "A Numerical Technique for Analysis of Wave Drag at Lifting Conditions," NASA TN D-3586, 1966.

Appendix A: WAVDRAG Input Files

Input File Description:

CONTROL:

- Digit 1: Specifies whether or not reference area will be input and used (1 or 0)
- Digit 2: Cambered wing (1), uncambered wing (-1), or no wing (0)
- Digit 3: Circular fuselage (-1), arbitrary fuselage (1), no fuselage (0)
- Digit 4: Pod (1), no pod (0)
- Digit 5: Fin (1), no fin (0)
- Digit 6: Canard (1), no canard (0)
- Digit 7: Configuration is symmetric w.r.t. plane of vertical tail (1), fuselage is symmetric (-1), no symmetry (0)
- Digit 8: Number of airfoil sections used to describe wing
- Digit 9: Number of stations on each airfoil where coordinates are given.
- Digit 10: Number of fuselage segments
- Digit 11: Number of coordinate sets per station given for first fuselage segment if not circular
- Digit 12: Number of stations for first fuselage segment
- Digit 13: Same as digit 11 for second segment
- Digit 14: Same as digit 12 for second segment
- Digit 15: Same as digit 11 for third segment
- Digit 16: Same as digit 12 for third segment
- Digit 17: Same as digit 11 for fourth segment
- Digit 18: Same as digit 12 for fourth segment
- Digit 19: Number of pods input
- Digit 20: Number of stations at which pod radii input
- Digit 21: Number of fins
- Digit 22: Number of stations at which coordinates are given for each fin airfoil
- Digit 23: Number of canards
- Digit 24: of stations at which coordinates are given for each canard airfoil

REFA: Reference wing area

XAF: Locations on each airfoil where ordinates are specified (in % chord)

WAFORG 1: First airfoil coordinates (x,y,z,chord l)

WAFORG 2: Second airfoil coordinates (x,y,z,chord l)

WAFORD 1-1: Ordinates of first airfoil

WAFORD 1-2: Ordinates of second airfoil

XFUS 1: Body axis coordinates of fuselage stations in segment 1 (nose is 0)

FUSARD 1: Cross sectional area of each station specified in XFUS in first segment

X FUS 2: Body axis coordinates of fuselage stations in segment 2

FUSARD 2: Cross sectional area of each station specified in XFUS in second segment

CASE 1:

Digits 1-3: Ordinates of second airfoil

Row 8

Columns 1-4: File description

Columns 5-8: Mach # x 1000

Entry 3: Number of intervals on x-axis (body axis)

Entry 4: Number of thetas

Entry 5: Number of restraint points ofr drag minimization

Entry 6: 1 if another configuration follows, 0 if only 1 configuration is given

Entry 7: Number of optimization cycles if optimization is turned on

Entry 8: Slope checking on (0), no slope checking (1)

Entry 9: Compute equivalent body areas, drags, (0), perform minimum calculations for wave drag (1)

XREST: x locations of fuselage restraint points, only applicable if optimization turned on

Appendix B: RLV & Trial 3b APAS Area Build-ups

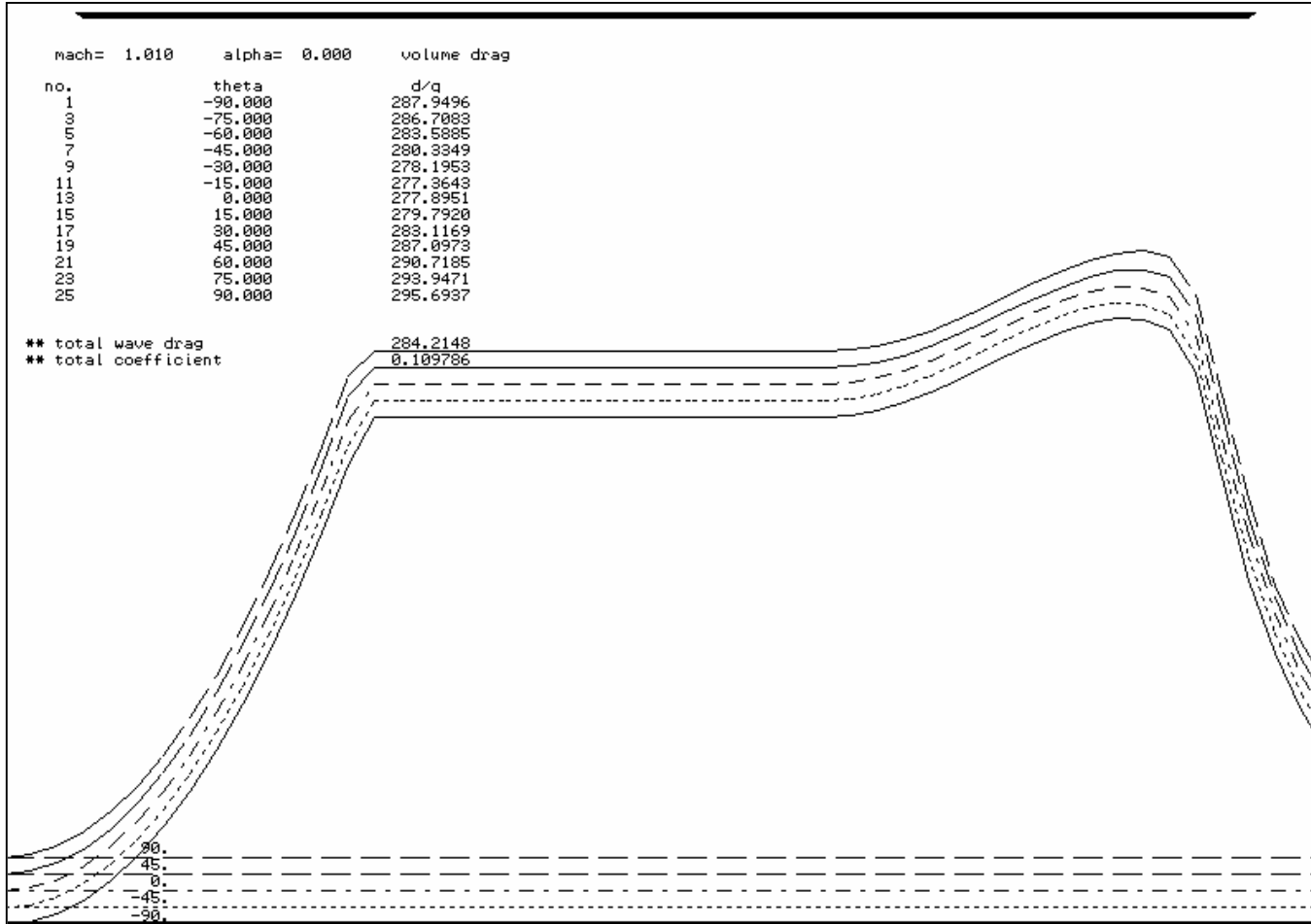


Figure 53. APAS Argus Area Build-up

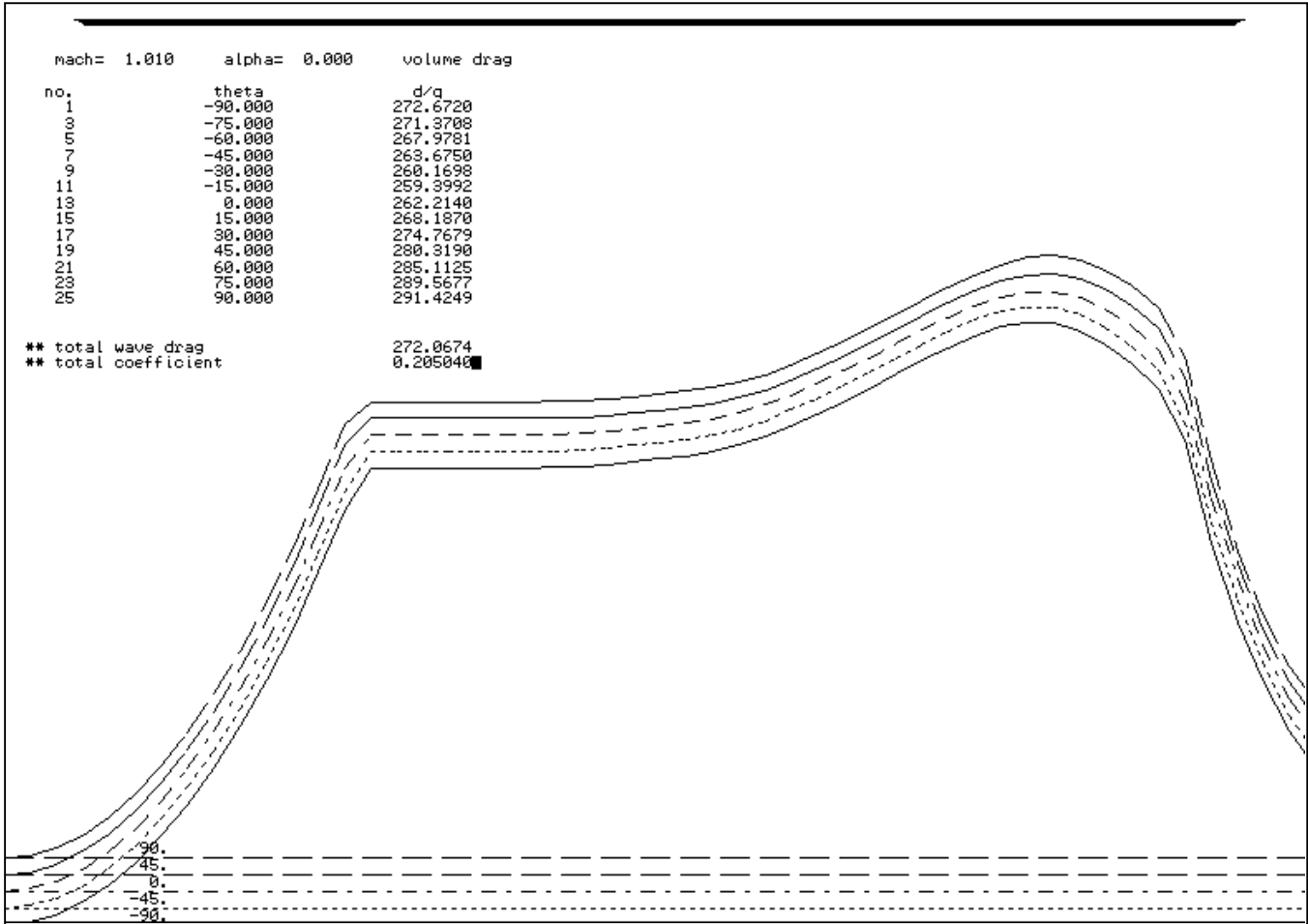


Figure 54. APAS Starsaber Area Build-up

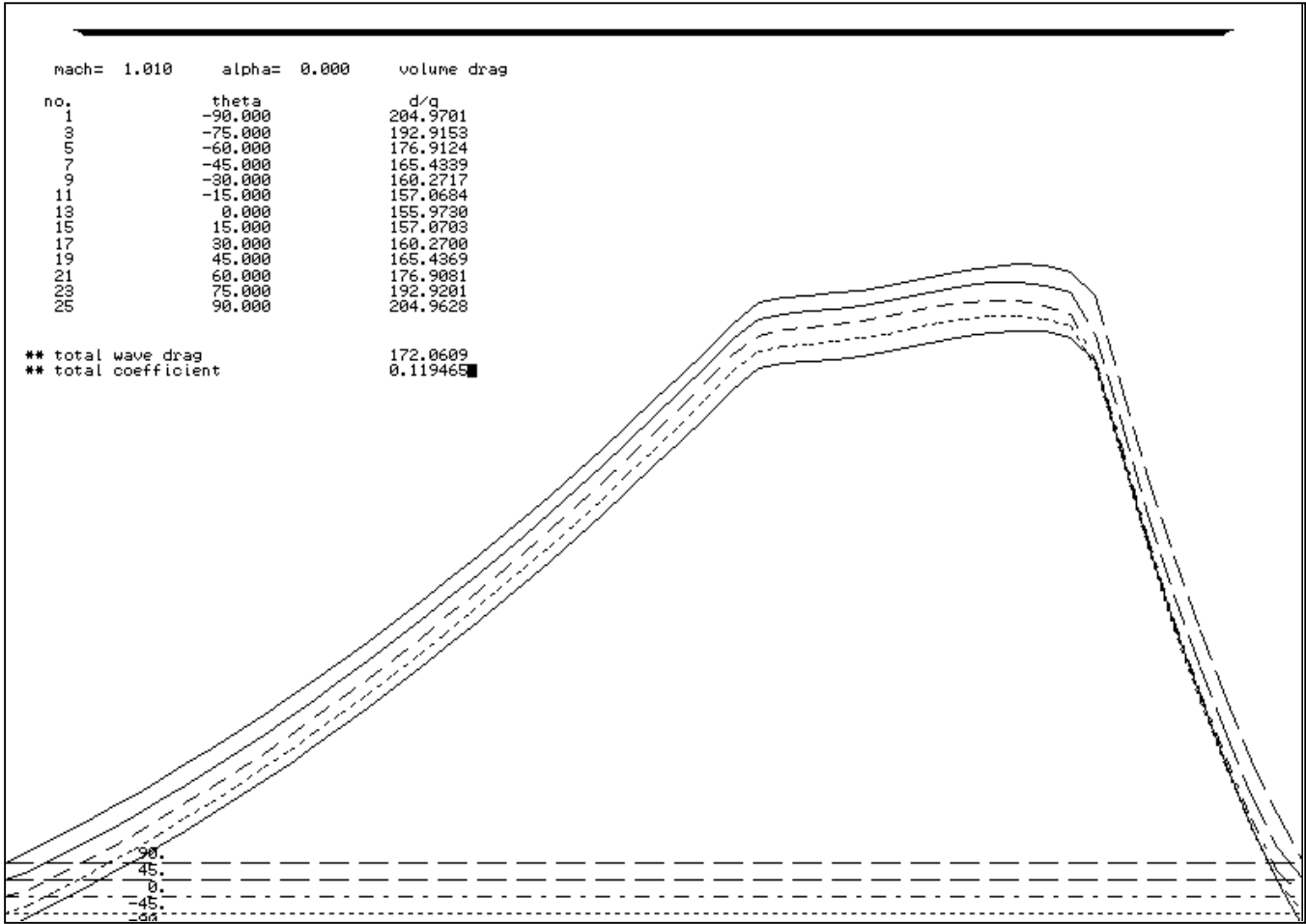


Figure 55. APAS Stargazer Area Build-up

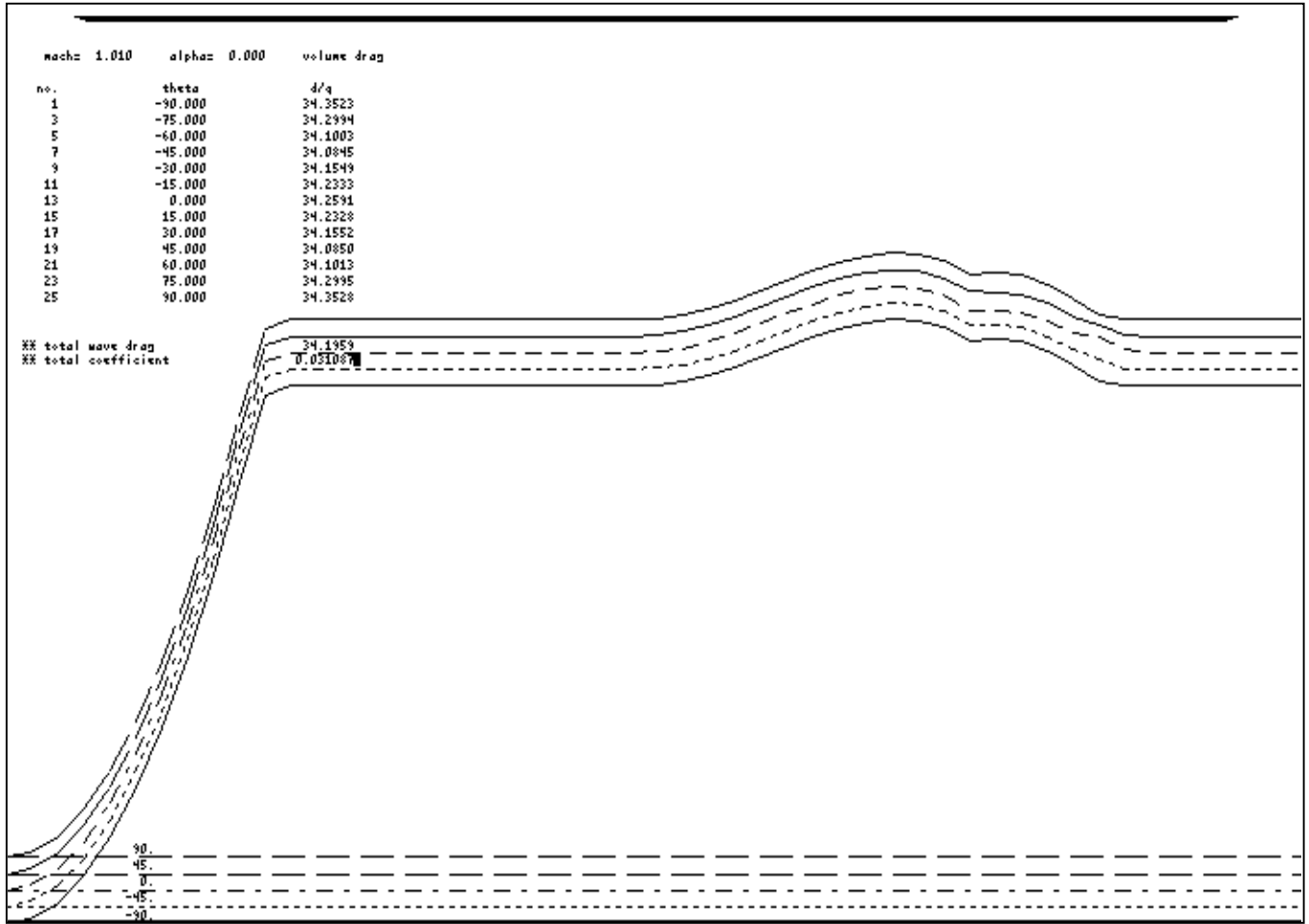


Figure 56: APAS Trial 3b Area Build-up

This document was created with Win2PDF available at <http://www.daneprairie.com>.
The unregistered version of Win2PDF is for evaluation or non-commercial use only.